JOURNAL OF GUIDANCE, CONTROL, AND DYNAMICS
Vol. 33, No. 3, May–June 2010

Evaluation of a Sliding Mode Fault-Tolerant Controller for the El Al Incident

H. Alwi* and C. Edwards†
University of Leicester, Leicester, England LE1 7RH, United Kingdom
and
O. Stroosma‡ and J. A. Mulder§
Delft University of Technology, 2600 GB Delft, The Netherlands

DOI: 10.2514/1.47442

This paper presents piloted flight simulator results associated with the El Al flight 1862 scenario, using a model-reference-based sliding mode control allocation scheme for fault-tolerant control. The proposed controller design was carried out without any knowledge of the type of failure and in the absence of any fault detection and isolation strategy. This is motivated by the fact that the flight crew were unaware of the losses of the right engines. For this reason, the control allocation scheme proposed uses (fixed) equal distribution of the control signals to all actuators (for both nominal situations and when a fault or failure occurs). This paper analyzes the scheme and determines the conditions under which closed-loop stability is retained. The results represent the successful real-time implementation of the proposed controller on a flight simulator, configured to represent a B747 aircraft. The evaluation results from the experienced pilots show that the proposed controller has the ability to position the aircraft for landing, both in a nominal scenario and in the El Al failure scenario. It is also shown that actuator faults and failures that occurred during the El Al incident can be handled directly without reconfiguring the controller.

Nomenclature

air, ail, aor, aol	=	inboard right, inboard left, outboard right, and outboard left ailerons
h_e, x_e, y_e	=	geometric Earth position along the z (altitude), x, and y axes, m
lat, long	=	lateral and longitudinal axes
p, q, r	=	roll, pitch, and yaw rates, rad/s
$\mathbb{R}$	=	field of real numbers and the set of strictly positive real numbers
s, σ	=	Laplace variable, sliding mode switching function
sp	=	spoiler
$u(t)$, $v(t)$	=	actual and virtual control input
V_{tas}	=	true air speed, m/s
α, β	=	angle of attack and sideslip angle, rad
$\bar{\lambda}(\cdot)$, $\underline{\lambda}(\cdot)$	=	largest and smallest eigenvalues
ϕ, θ, ψ	=	roll, pitch, and yaw angles, rad
$\|\cdot\|$	=	Euclidean norm (vectors) or induced spectral norm (matrices)

I. Introduction

LESSONS learned from previous incidents suggest that, in many cases, damaged/faulty aircraft are still flyable and controllable with some level of performance, which makes it possible for the pilot to safely land the aircraft in an emergency situation. For example, in Sioux City, Iowa, in 1989, Flight 232 (DC-10) suffered tail engine failure that caused the total loss of hydraulics (Burcham et al. [1] and Gero [2]). In Detroit, Michigan, in October 2004, the Kalita Air freighter (B747) shed engine no. 1, but the crew managed to land safely without any casualties. Whilst in Baghdad, in November 2003, the DHL freighter (A300B4) was hit by a missile on its left wing and lost all hydraulics, but it still landed safely (Burcham et al. [1]). This has also been shown by a successful program carried out by NASA on propulsion-controlled aircraft (as described in the work of Burcham et al. [3–5], Tucker [6], and Burken et al. [7], which considers MD-11, B747, C17, and F15 aircraft), which showed that the controllers developed during the study helped the pilots to land the aircraft safely in the event of total hydraulic loss (Tucker [6]). An independent investigation of the El Al flight 1862 (which crashed into an apartment building in Bijlmermeer, Amsterdam), conducted by Delft University (Smaili and Mulder [8]), suggested that there was still some maneuvering capability associated with the damaged aircraft. This is backed up by an early publication on fault-tolerant control (FTC) by Maciejowski and Jones [9], which showed that it was possible to control the damaged aircraft via a model predictive control (MPC) scheme (although Maciejowski and Jones [9] assume an exact postdamage model is available). Subsequent work by Hennig and Balas [10] on MPC for FTC also considers the El Al 1862 scenario.

The El Al flight 1862 scenario was used as the basis for the Group for Aeronautical Research and Technology in Europe (GARTEUR) Flight Mechanics Action Group 16 (FM–AG16), which explored and assessed the use of modern fault detection and isolation (FDI) and FTC strategies to improve flight safety. Recent papers from the GARTEUR FM-AG16 program include Lombaerts et al. [11] (which uses adaptive nonlinear dynamic inversion), whereas the paper by Stroosma et al. [12] discusses simulator evaluations of different FM-AG16 controllers.

The work in Shtessel et al. [13] and Wells and Hess [14] provides practical examples of the combination of sliding mode control (SMC) and control allocation (CA) for FTC. These papers exploit the inherent robustness of sliding modes, which when integrated with CA, allow total failures of certain actuators to be accommodated.

Presented as Paper 7157 at the AIAA Guidance, Navigation, and Control Conference and Exhibit, Honolulu, HI, 18–21 August 2009; received 30 September 2009; revision received 13 December 2009; accepted for publication 25 January 2010.

*Research Associate, Control and Instrumentation Research Group, Engineering Department.

†Reader, Control and Instrumentation Research Group, Engineering Department.

‡Research Assistant, International Research Institute for Simulation, Motion and Navigation. Member AIAA.

§Professor, Control and Simulation Division, Faculty of Aerospace Engineering. Member AIAA.

More recently, in Alwi and Edwards [15,16], a SMC allocation scheme was proposed. Easily testable conditions were developed to guarantee the stability of the closed-loop system subject to a certain class of actuator faults (which will be precisely described later in the paper). The scheme in Alwi and Edwards [16] uses a control law that depends on (an estimation of) the efficiency/effectiveness of the actuators.

The results in this paper are the outcome of the controller evaluation flight testing campaign and the GARTEUR FM-AG16 final workshop at Delft University, The Netherlands. The results presented represent the successful real-time implementation of the proposed sliding mode controller on the International Research Institute for Simulation, Motion, and Navigation's (SIMONA's) six-degree-of-freedom (DOF) motion flight simulator. The results presented were obtained by airline and test pilots with experience covering B747, B767, A330, and Citation II aircraft, on the El Al flight 1862 (Bijlmermeer incident) scenario, which is one of the case studies associated with the GARTEUR FM-AG16.

The controller that has been used is a modification of the model-reference sliding mode controller proposed by Alwi and Edwards [15]. The model-reference tracking framework chosen in this paper has advantageous features, especially the absence of integrators, when compared with the controller in Alwi et al. [17]. The absence of integrators eliminates the dangers of controller windup in the face of saturation and rate limits being exceeded during faults, failures, or structural damage. Another advantageous feature of the model-reference framework is that the performance specifications are predefined and represented in terms of an ideal-transfer-function response.

In this paper, the situation that occurred during the El Al flight 1862, whereby the flight crew were unaware that engine nos. 3 and 4 had separated from the wing (despite reporting the loss of thrust from both engines), will be assumed. This is the motivation for the tests carried out in this paper, which are all performed under the assumption that the type of failure is unknown and in the absence of any FDI or fault reconstruction strategy. Therefore, the controller has been designed with no knowledge of the failure and the damage to the airframe. Because there is no FDI and no actuator effectiveness estimation available, a fixed CA approach (as described in Alwi et al. [17]) will be used. The fixed CA scheme is sufficient to access the remaining available control surfaces' capability, and it passively controls the aircraft, exploiting the robust properties of the sliding mode controllers to ensure stability and some nominal performance. (Here, passive refers to passive fault-tolerant controllers, which are defined by Patton [18] and Zhang and Jiang [19] as controllers that are robust and insensitive to certain faults without the use of online fault information and without requiring controller reconfiguration.)

The controller has been designed as an autopilot that receives pilot set points from the mode control panel (MCP) in order to change roll, sideslip, flight-path angle (FPA), and speed. An outer-loop heading, an altitude change/hold, and an instrument landing system (ILS) landing approach have also been included to provide assistance to position the aircraft for landing.

II. Test Facilities of the International Research Institute for Simulation, Motion, and Navigation

The FTLAB747 software (representing a high-fidelity 6-DOF rigid-body aerodynamic model of the B747-100/200 aircraft), which runs on MATLAB®, has been developed by several researchers (van der Linden [20], Smaili [21], and Marcos and Balas [22]). The 77-state FTLAB747 model consists of the 12 rigid-body states and incorporates detailed dynamical models of the sensors and actuators together with realistic position and rate limits. This software has been used as a realistic platform to test FTC and FDI schemes by many researchers (e.g., Hennig and Balas [10], Marcos and Balas [23], Marcos et al. [24], Szaszi et al. [25], and Zhou et al. [26]). In its latest incarnation, it has been used as part of the GARTEUR FM-AG16 group as a benchmark (and described in detail Smaili et al. [27]).

The SIMONA research simulator (SRS), shown in Fig. 1, is a pilot-in-the-loop flight simulator with motion capabilities, operated by Delft University of Technology. It provides researchers with a powerful tool that can be adapted to various uses (Stroosma et al. [28]). The simulator's flexible software architecture and high-fidelity cueing environment allow the integration of the aircraft model from Smaili et al. [27]. Its inputs and outputs were standardized to fit the SRS software environment, and the SIMULINK aircraft model was converted to C code using the Real-Time Workshop. Finally, the model was integrated with the pilot controls, the aircraft instruments (Fig. 1b), and other cueing devices of the SRS (i.e., outside visual and motion systems). On the flight deck of the SRS, the evaluation pilot was presented with flight instruments representative of a B747 aircraft, a control column with appropriate feel system dynamics, a central pedestal with dual-engine controls, a MCP for controlling the autopilot, and a wide collimated view on a virtual outside world. The simulator's motion system was tuned to give the pilot realistic inertial motion cues in nominal and failure conditions.

III. El Al Flight 1862: The Incident

On 04 October 1992, the El Al flight 1862 freighter aircraft, a Boeing 747-200 (on a scheduled flight from John F. Kennedy International Airport, New York, to Tel Aviv, Israel) departed from Schiphol Airport, Amsterdam, after a refuelling and crew change. Shortly after takeoff, as the aircraft reached an altitude of about 6500 ft, the pilots transmitted an emergency call. The crew reported a fire in engine no. 3 and the loss of thrust in engine nos. 3 and 4 as the aircraft was turning to the right. As described in the incident report by The Netherlands Aviation Safety Board [29], the pilots were operating under extreme workload conditions, trying to control the aircraft. Straight and level flight required full-left (positive) rudder pedal deflection and 60 to 70% maximum lateral control (the wheel almost full to the left) [29]. A series of right-hand turns were performed in order to land on runway 27. The first attempt to intercept the localizer (LOC) and align for the final approach course was unsuccessful, as the aircraft overshot the LOC. Shortly after, the crew reported that engine nos. 3 and 4 were inoperative, and they reported a problem on the wing flaps. During the second attempt to

a) Outside view b) Flight deck view

Fig. 1 SRS.

intercept the LOC, heading and altitude changes to 310 deg and 1500 ft, respectively, were requested. The flight crew immediately reported control difficulties. The aircraft crashed 13 km east of Schiphol Airport into an apartment building in Bijlmermeer, a suburb of Amsterdam. Further details on the incident can be found in the accident report by The Netherlands Aviation Safety Board [29].

It is important to highlight that, for the duration of the incident, the flight crew was unaware that engine nos. 3 and 4 had separated from the wing, despite reporting loss of thrust from both engines. Unknown to the flight crew, the inboard fuse pin that held engine no. 3 to the pylon broke due to fatigue. This caused engine no. 3 and its pylon to separate from the right wing shortly after takeoff, causing damage to the leading edge of the right wing. (The role of the fuse pin is to allow the engine to separate from the wing under a strong impact, which occurs in the event of a crash or hard landing, in order to protect the fuselage from engine fire.) The shedding of engine no. 3 from the right wing in an outboard and rearward direction resulted in a collision with engine no. 4 (see Fig. 2), causing it and its pylon to separate from the wing. Figure 2 illustrates the estimated damage thought to have occurred on the right wing. (Smaili et al. [27] argue that, although only engine no. 2 was shed in the accident in Anchorage, Alaska, on 31 March 1993, the amount of damage on the wing's leading edge, as shown in Fig. 3, was probably indicative of the damage inflicted on the El Al 1862 wing.)

The damage and the effect on the El Al flight 1862 aircraft can be summarized as as follows:

1) The aircraft systems experienced a) the loss of hydraulic system nos. 3 and 4 and b) a right (positive) yawing moment due to asymmetric thrust from engine nos. 1 and 2.

2) A mass reduction of about 10 tons, resulting from the loss of engine nos. 3 and 4 (and the pylons) and lateral CG displacement (toward the left wing) due to the loss of the engines.

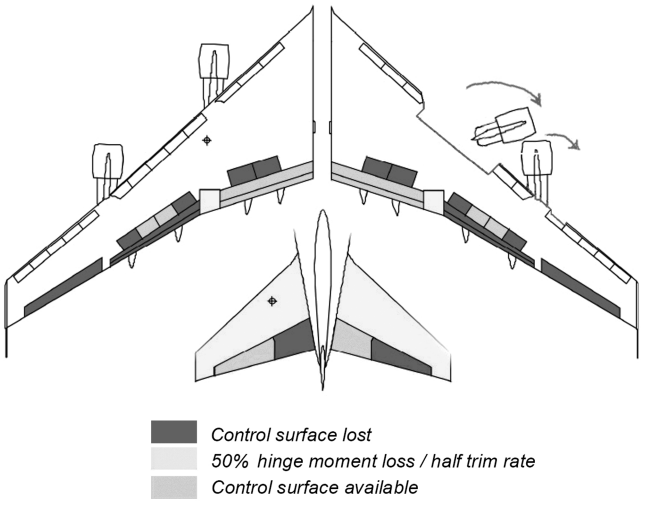

Fig. 2 El Al flight 1862: actuator fault/failure and structural damage (adapted from the El Al incident report [29] and Smaili et al. [27]).

3) Aerodynamic effect changes, including a) a lift loss on the right wing and additional drag caused by the damaged leading edge, b) changes to the roll pitch and yaw moment caused by the wing damage, and c) a loss of efficiency of the right inboard aileron and spoilers 10 and 11, due to airflow disruption caused by the damaged right-wing leading edge.

Figure 2 summarizes the losses and the remaining functional control surfaces (due to the loss of hydraulic system nos. 3 and 4, as described in the incident report [29]). The control surfaces lost due to the failure of hydraulic system nos. 3 and 4 were the outboard trailing-edge flaps; the right outboard aileron; spoilers 1, 4, 5, 8, 9, and 12; the left inboard elevator; and the right outboard elevator. The control surfaces that are still functional but affected by the loss of the hydraulic systems are the horizontal stabilizer, the inboard ailerons (both at half rate), and the lower rudder (lag). Although the right inboard aileron and spoilers 10 and 11 remain fully functional, the airflow disruption, resulting from the damage to the leading edge of the right wing, reduces their aerodynamic efficiency and their capacity to provide a roll moment. The only fully functional control surfaces are the inboard trailing-edge flaps, spoilers 2 and 3, the left outboard elevator, and the right inboard elevator.

Early FTC studies on El Al flight 1862 by Maciejowski and Jones [9] showed that it is possible to control the damaged aircraft (although Maciejowski and Jones [9] assumed an accurate model of the damaged aircraft was available to the controller, either from an FDI scheme or from system identification/estimation).

IV. Model-Reference Sliding Mode Control Allocation Scheme

This paper considers a situation in which a fault associated with the actuators develops in a system. It will be assumed that the system, subject to actuator faults or failures, can be written as

$$\dot{x}(t) = [A + A^{\delta}(t)]x(t) + Bu(t) - BK(t)u(t) + BK(t)d(t) \quad (1)$$

where $A \in \mathbb{R}^{n_x \times n_x}$ and $B \in \mathbb{R}^{n_x \times n_u}$. Structural damage is described by a change in the system matrix A, represented by $A^{\delta}(t)$. The effectiveness gain is

$$K(t) := \text{diag}[k_1(t), \ \ldots \ , k_{n_u}(t)]$$

where the $k_i(t)$ are scalars satisfying $0 \leq k_i(t) \leq 1$. These scalars model a decrease in effectiveness of a particular actuator. If $k_i(t) = 0$, the ith actuator is working perfectly, whereas if $k_i(t) > 0$, a fault is present and, if $k_i(t) = 1$, the actuator has failed completely. The exogenous signal $d(t)$ represents a disturbance that may impact on the system as a result of a fault/failure: for example, the moment generated by a control surface that has stuck in a nonneutral position in control channel i could be modeled as $k_i = 1$ and $d_i \neq 0$.

Remark: The control law based on the model in Eq. (1) (i.e., from a linearization about an operating condition) is only likely to be applicable over part of the flight envelope, and it will rely on the robust properties of the controller.

In most CA strategies, the control signal is distributed equally among all the actuators (Shin et al. [30], Shtessel et al. [13], and Wells

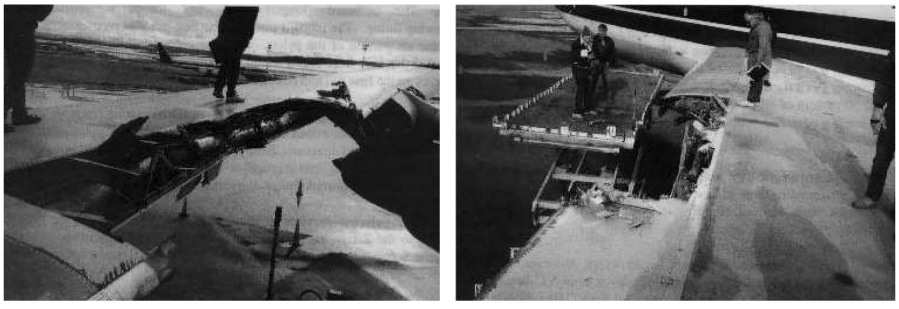

a) **b)**

Fig. 3 Wing damage due to separation of engine no. 2, Anchorage, 1993 (adapted from Smaili et al. [27]).

and Hess [14]) or distributed based on the limits (position and rate) of the actuators (Härkegård and Glad [31]). In papers by Alwi and Edwards [15,16], information about $K(t)$ has been incorporated into the allocation algorithm through a weighting matrix W, so that the control is redistributed to the remaining healthy actuators when faults/failures occur. In this paper, the CA strategy is based on the widely used approaches from the literature (i.e., fixed and equal distribution of the control signals). This is motivated by the fact that the information about $K(t)$ in Eq. (1) is not always available and mirrors what happened during the El Al flight 1862 scenario.

The input distribution matrix B from Eq. (1) is assumed to have been reordered and partitioned as

$$B = \begin{bmatrix} B_1 \\ B_2 \end{bmatrix} \tag{2}$$

where $B_1 \in \mathbb{R}^{(n_u - n_v)\times n_u}$ and $B_2 \in \mathbb{R}^{n_v \times n_u}$ have rank $n_v < n_u$. The partition is in keeping with the notion of splitting the control law from the CA task (Härkegård [32] and Beck [33]). In aircraft systems, the overall control objectives can be successfully achieved by generating appropriate moments about the principal axes by use of the control surfaces (Härkegård [32] and Beck [33]). In this paper, B_2 is associated with the equations of angular acceleration in roll, pitch, and yaw [31]; although, in principle, this can be extended to other systems that may have no partition of the control law (Beck [33]). In this paper, the matrix B_2 represents the dominant contribution of the control action on the system, whereas B_1 generally will have elements of small magnitude when compared with $\|B_2\|$. This formulation is more general when compared with earlier work (for example, by Shin et al. [30]), in which it is assumed that $B_1 = 0$. It will be assumed that, without loss of generality, the states of the system in Eq. (1) have been transformed, so that $B_2 B_2^T = I_{n_v}$; therefore, $\|B_2\| = 1$. Let the virtual control[¶] be given by

$$\nu(t) := B_2 u(t) \tag{3}$$

so that

$$u(t) = B_2^{\dagger} \nu(t) \tag{4}$$

where the right pseudoinverse is chosen as

$$B_2^{\dagger} := B_2^T \tag{5}$$

[In linear algebraic terms, a pseudoinverse is a generalization of the inverse matrix (Horn and Johnson [34] and Penrose [35]).] For a nonsquare matrix, a perfect inverse is not available; therefore, an approximate inverse (i.e., a pseudoinverse) is used. Here, $B_2^{\dagger}$ has the property that $B_2 B_2^{\dagger} = I_{n_v}$ while solving the optimization problem in Eq. (6), next. The pseudoinverse in Eq. (5) arises from the optimization problem,

$$\min_u \|u\|^2 \tag{6}$$

subject to

$$B_2 u = \nu$$

Remark: Note that, compared with Eq. (6), there exist more general-optimization-problem formulations for CA (see, for example, Enns [36] and Durham [37]). However, in the context of this paper, especially for the real-time SIMONA implementation, it will be shown that one of the key issues is the onboard computational constraint. By adopting a simple optimization approach, as in Eq. (6), the real-time computational constraints can be met, thus allowing successful real-time implementation.

In the event of faults/failures or structural damage to the aircraft, equilibrium needs to be achieved first. The damage on the wing in the El Al incident caused a nonzero roll, pitch, and yaw moment. Therefore, in order to achieve equilibrium, control surface trims are required. During the actual incident, the pilots managed to achieve an equilibrium condition of straight and level flight by manipulating the control surfaces. In this paper, the changes in the trim condition will be automatically compensated for by the controller, and no pilot input is required. In terms of the stability analysis that follows, the effect of the exogenous disturbance $d(t)$ from Eq. (1) is ignored. Clearly, this external signal does not formally affect the stability or otherwise of the closed-loop system associated with Eq. (1); although, of course, it affects the closed-loop performance of the system. In the real system, it will directly affect the trim points and the flight envelope of the damaged aircraft. In the following stability analysis, $d \equiv 0$. The development that follows is similar in spirit to Alwi and Edwards [16], but it is different in detail because of the model-reference setting. Using Eqs. (4) and (5), it can be shown that Eq. (1) can be written as

$$\dot{x}(t) = [A + A^{\delta}(t)]x(t) + \underbrace{\begin{bmatrix} B_1 B_2^T \\ I \end{bmatrix}}_{B_v} \nu(t) - \underbrace{\begin{bmatrix} B_1 K B_2^T \\ B_2 K B_2^T \end{bmatrix}}_{\bar{B}_k} \nu(t) \tag{7}$$

In the nominal fault-free case, $A^{\delta}(t) = 0$, $K = 0$, and $\bar{B}_k$ in Eq. (7) is zero. Consider a reference model defined as

$$\dot{x}_m(t) = A_m x_m(t) + B_m y_d(t) \tag{8}$$

where $y_d(t)$ is the reference signal and $A_m \in \mathbb{R}^{n_x \times n_x}$ and $B_m \in \mathbb{R}^{n_x \times n_v}$ with A_m are stable. Define

$$e(t) = x(t) - x_m(t) \tag{9}$$

Therefore, from Eqs. (7) and (8), the error system

$$\begin{aligned} \dot{e}(t) = {} & [A + A^{\delta}(t)]e(t) + [A^{\delta}(t) + A - A_m]x_m(t) \\ & + B_v \nu(t) - \bar{B}_k \nu(t) - B_m y_d(t) \end{aligned} \tag{10}$$

The matrices A_m and B_m in Eq. (8) represent the reference model that defines the required closed-loop system performance. Here, the reference model matrices A_m and B_m are chosen as

$$A_m = A + B_v F; \qquad B_m = B_v G \tag{11}$$

Other approaches to define the ideal model can be adopted (see, for example, Landau [38], Landau and Courtoil [39], and Monopoli and Subbarao [40]), but here the formulation that has been traditionally incorporated within a sliding mode framework has been employed (Broussard and O'Brien [41] and Zinober et al. [42]). The matrices F and G represent the feedback and feedforward terms that define the reference model. Based on these matrices, define a feedforward signal as

$$\nu_m(t) := F x_m(t) + G y_d(t) \tag{12}$$

Sliding mode techniques (Utkin [43] and Edwards and Spurgeon [44]) will now be used to synthesize $\nu(t)$. The control objective seeks to minimize the error between the reference model and the virtual controlled plant (A, B_v) in Eq. (7). Define a so-called switching function, σ: $\mathbb{R}^{n_x} \to \mathbb{R}^{n_v}$, to be

$$\sigma(t) = S e(t) \tag{13}$$

where the design parameter $S \in \mathbb{R}^{n_v \times n_x}$, and $\det(SB_v) \neq 0$ by construction. Let $\mathcal{S}$ be the hyperplane defined by $\mathcal{S} = \{e(t) \in \mathbb{R}^{n_x} : Se(t) = 0\}$. If a control law can be developed that forces the closed-loop trajectories onto the surface $\mathcal{S}$ in finite time and constrains the states to remain there, then an ideal sliding motion is said to have been attained (Edwards and Spurgeon [44]). The sliding surface will be designed, based on the nominal no-fault condition ($K = 0$). Using Eq. (11), Eq. (10) can be rewritten as

[¶]In this context, virtual control refers to a fictitious control input, which is used for control law design, and not the actual plant inputs. The mapping between the virtual inputs and the true inputs is the problem of CA (Härkegård [32]).

$$\dot{e}(t) = [A + A^{\delta}(t)]e(t) + A^{\delta}(t)x_m(t) - \bar{B}_k\nu(t) + B_{\nu}[\nu(t)\underbrace{-Fx_m(t) - Gy_d(t)}_{-\nu_m(t)}] \tag{14}$$

where B_{ν} and $\bar{B}_k$ are defined in Eq. (7). A coordinate transformation $e \mapsto T_r e(t) = \hat{e}(t)$ is introduced to obtain regular form (Utkin [43] and Edwards and Spurgeon [44]). If

$$T_r := \begin{bmatrix} I & -B_1B_2^T \\ 0 & I \end{bmatrix} \tag{15}$$

then by using similar arguments to those in Alwi and Edwards [45], Eq. (14) becomes

$$\dot{\hat{e}}(t) = (\hat{A} + \hat{A}^{\delta})\hat{e}(t) + \hat{A}^{\delta}\hat{x}_m(t) + \underbrace{\begin{bmatrix} 0 \\ I \end{bmatrix}}_{\hat{B}_{\nu}}[\nu(t) - \nu_m(t)] - \begin{bmatrix} -B_1B_2^N(I-K)B_2^T \\ I - B_2(I-K)B_2^T \end{bmatrix}\nu(t) \tag{16}$$

where $\hat{A} := T_rAT_r^{-1}$, $\hat{A}^{\delta} := T_rA^{\delta}T_r^{-1}$, and $\hat{x}_m = T_rx_m(t)$. The projection operator

$$B_2^N := (I - B_2^TB_2) \tag{17}$$

Because, by construction, the matrix $B_2B_2^T = I_l$, it follows that $B_2^NB_2^T = (I - B_2^TB_2)B_2^T = 0$. Therefore, the last term in Eq. (16) is zero in a fault-free case ($K = 0$), but it is treated as (unmatched) an uncertainty when $K \neq 0$. Define

$$W := I - K \tag{18}$$

and write

$$B_2^+ := WB_2^T(B_2WB_2^T)^{-1} \tag{19}$$

As shown in Stewart [46], there exists a scalar γ_0 that is finite and independent of W, such that

$$\|B_2^+\| = \|WB_2^T(B_2WB_2^T)^{-1}\| < \gamma_0 \tag{20}$$

for all $W = \text{diag}(w_1, \ldots, w_{n_u})$, such that $0 < w_i \leq 1$.

The development now diverges from the exposition in Alwi and Edwards [16] because of the inclusion of the parametric uncertainty not analyzed in Alwi and Edwards [16]. A virtual control law will now be designed, based on the nominal fault-free system in which the last term in Eq. (16) is zero. In the $\hat{e}(t)$ coordinates, a suitable choice for the sliding surface matrix is

$$\hat{S} = ST_r^{-1} = [M \quad I] \tag{21}$$

where $M \in \mathbb{R}^{n_{\nu} \times (n_x - n_{\nu})}$ represents design freedom. Introduce another transformation $(\hat{e}_1, \hat{e}_2) \mapsto (\hat{e}_1, \sigma) = \tilde{e}$ associated with

$$T_{\sigma} = \begin{bmatrix} I & 0 \\ M & I \end{bmatrix} \tag{22}$$

Equation (16) then becomes

$$\begin{bmatrix} \dot{\hat{e}}_1(t) \\ \dot{\sigma}(t) \end{bmatrix} = \begin{bmatrix} \tilde{A}_{11} + \tilde{A}_{11}^{\delta} & \tilde{A}_{12} + \tilde{A}_{12}^{\delta} \\ \tilde{A}_{21} + \tilde{A}_{21}^{\delta} & \tilde{A}_{22} + \tilde{A}_{22}^{\delta} \end{bmatrix} \begin{bmatrix} \hat{e}_1(t) \\ \sigma(t) \end{bmatrix} + \begin{bmatrix} \tilde{A}_1^{\delta} \\ \tilde{A}_2^{\delta} \end{bmatrix} \tilde{x}_m(t) + \begin{bmatrix} 0 \\ I \end{bmatrix}[\nu(t) - \nu_m(t)] - \begin{bmatrix} -B_1B_2^NWB_2^T \\ I - MB_1B_2^NWB_2^T - B_2WB_2^T \end{bmatrix}\nu(t) \tag{23}$$

In the previous equation, $\tilde{A}_{11} := \hat{A}_{11} - \hat{A}_{12}M$ and $\tilde{A}_{21} := M\tilde{A}_{11} + \hat{A}_{21} - \hat{A}_{22}M$, where

$$\hat{A} = \begin{bmatrix} \hat{A}_{11} & \hat{A}_{12} \\ \hat{A}_{21} & \hat{A}_{22} \end{bmatrix} \tag{24}$$

and

$$\tilde{A}^{\delta} = \begin{bmatrix} \tilde{A}_{11}^{\delta} & \tilde{A}_{12}^{\delta} \\ \tilde{A}_{21}^{\delta} & \tilde{A}_{22}^{\delta} \end{bmatrix} = \begin{bmatrix} \tilde{A}_1^{\delta} \\ \tilde{A}_2^{\delta} \end{bmatrix}$$

and $\text{col}(\tilde{x}_{m_1}, \tilde{x}_{m_2}) = \tilde{x}_m = T_{\sigma}\hat{x}_m$.

If a control law can be designed to induce a sliding motion, then during sliding, $\dot{\sigma}(t) = \sigma(t) = 0$, and the equivalent control necessary to maintain sliding is obtained from solving for $\nu_{\text{eq}}(t)$ from the lower equations of Eq. (23) to give

$$\nu_{\text{eq}}(t) = (B_2WB_2^T)^{-1}(I + MB_1B_2^NB_2^+)^{-1} \times [-(\tilde{A}_{21} + \tilde{A}_{21}^{\delta})\hat{e}_1(t) + \nu_m(t) - \tilde{A}_2^{\delta}\tilde{x}_m(t)] \tag{25}$$

where B_2^N and B_2^+ are defined in Eqs. (17) and (19), respectively. Assume the sliding surface matrix M has been designed, so that $\tilde{A}_{11} := \hat{A}_{11} - \hat{A}_{12}M$ is stable, and $\|MB_1B_2^NB_2^+\| < 1$ for all $0 < W \leq I$.

Remark: $\|MB_1B_2^NB_2^+\| < 1$ guarantees the inverse in Eq. (25) exists and uses the boundedness result from Eq. (20). If the inverse in Eq. (25) cannot be guaranteed to exist, the sliding motion cannot be guaranteed. Inequality $\|MB_1B_2^NB_2^+\| < 1$ depends on both the hyperplane design (through M) and the faults/failures, because B_2^+ depends directly on W.

If (A, B_{ν}) is controllable, then $(\hat{A}_{11}, \hat{A}_{12})$ from Eq. (24) is controllable (Edwards and Spurgeon [44]), and so M can be chosen to make $\hat{A}_{11} - \hat{A}_{12}M$ stable. Substituting Eq. (25) into the top partition of Eq. (23) yields the following reduced-order system, which governs the sliding motion:

$$\dot{\hat{e}}_1(t) = [(\tilde{A}_{11} + \tilde{A}_{11}^{\delta}) - B_1B_2^NB_2^+(I + MB_1B_2^NB_2^+)^{-1} \times (\tilde{A}_{21} + \tilde{A}_{21}^{\delta})]\hat{e}_1(t) + B_1B_2^NB_2^+(I + MB_1B_2^NB_2^+)^{-1} \times [\nu_m(t) - \tilde{A}_2^{\delta}\tilde{x}_m(t)] \tag{26}$$

In the event of faults/failures, stability of the system in Eq. (26) (which depends on W through B_2^+) needs to be established.

A. Stability Analysis

The stability of the sliding mode is dependent on the reduced-order system in Eq. (26). Because, by construction, the reference model is stable for a bounded signal $y_d(t)$, the signal $x_m(t)$ is bounded, and hence ν_m from Eq. (12) is bounded. Therefore, the stability of the reduced-order system that governs the sliding motion depends on

$$\dot{\hat{e}}_1(t) = [(\tilde{A}_{11} + \tilde{A}_{11}^{\delta}) - B_1B_2^NB_2^+(I + MB_1B_2^NB_2^+)^{-1} \times (\tilde{A}_{21} + \tilde{A}_{21}^{\delta})]\hat{e}_1(t) \tag{27}$$

In a fault-free case, $W = I, \tilde{A}_{11}^{\delta} = \tilde{A}_{21}^{\delta} = 0$, and the system in Eq. (27) collapses to $\dot{\hat{e}}_1(t) = \tilde{A}_{11}\hat{e}_1(t)$, which is the nominal sliding mode reduced-order system for which M has been designed to guarantee stability. In the case when actuator faults/failures occur but there is no structural damage, $\tilde{A}^{\delta} = 0 \Rightarrow \tilde{A}_{11}^{\delta} = \tilde{A}_{21}^{\delta} = 0$, and the stability analysis (which was discussed in Alwi and Edwards [16]) applies.

Assume that $\tilde{A}_{21}^{\delta} = \tilde{\Delta}_2(t)\tilde{A}_{21}$, where $\tilde{\Delta}_2(t) \in \mathbb{R}^{n_{\nu} \times n_{\nu}}$, and $\tilde{\Delta}_2(t)$ is unknown but bounded. Also assume that $\tilde{A}_{11}^{\delta} = \tilde{G}\tilde{\Delta}_1(t)\tilde{H}$, where $\tilde{G} \in \mathbb{R}^{(n_x - n_{\nu}) \times n_y}$, $\tilde{H} \in \mathbb{R}^{n_y \times (n_x - n_{\nu})}$, and $\tilde{\Delta}_1(t) \in \mathbb{R}^{n_y \times n_y}$. Here, the matrices $\tilde{G}$ and $\tilde{H}$ are assumed to be known, whereas $\tilde{\Delta}_1(t)$ is unknown but bounded. Therefore, Eq. (27) can be represented by

$$\dot{\hat{e}}_1(t) = [(\tilde{A}_{11} + \tilde{G}\tilde{\Delta}_1\tilde{H}) - B_1B_2^NB_2^+(I + MB_1B_2^NB_2^+)^{-1} \times (I_l + \tilde{\Delta}_2)\tilde{A}_{21}]\hat{e}_1(t) \tag{28}$$

To facilitate the subsequent analysis, define

$$\tilde{P}(s) := \begin{bmatrix} \tilde{H} \\ \tilde{A}_{21} \end{bmatrix} (sI - \tilde{A}_{11})^{-1} \begin{bmatrix} \tilde{G} & -B_1 B_2^N \end{bmatrix} \tag{29}$$

where s represents the Laplace variable. By construction, the transfer function $\tilde{P}(s)$ is stable. Suppose

$$\gamma_1 := \|MB_1 B_2^N\| \tag{30}$$

and assume that M has been designed so that $\tilde{A}_{11} = (\hat{A}_{11} - \hat{A}_{12}M)$ is stable and $\gamma_1 \leq \frac{1}{\gamma_0}$, where γ_0 is defined in Eq. (20). Suppose that

$$\|I + \tilde{\Delta}_2(t)\| \leq \gamma_3 \tag{31}$$

where $\gamma_3 > 1$ is a known scalar. It can be shown that

$$\begin{aligned} &\|B_2^+ (I + MB_1 B_2^N B_2^+)^{-1} (I + \tilde{\Delta}_2)\| \\ &\quad \leq \|B_2^+\| \|(I + MB_1 B_2^N B_2^+)^{-1}\| \|(I + \tilde{\Delta}_2)\| \leq \frac{\gamma_0 \gamma_3}{1 - \gamma_1 \gamma_0} \end{aligned} \tag{32}$$

because

$$\|(I + MB_1 B_2^N B_2^+)^{-1}\| \leq (1 - \|MB_1 B_2^N\| \|B_2^+\|)^{-1} \leq (1 - \gamma_1 \gamma_0)^{-1}$$

Scale $\tilde{G}$ and $\tilde{H}$ appropriately, so that

$$\max_{\tilde{\Delta}_1} \|\tilde{\Delta}_1(t)\| = \frac{\gamma_0 \gamma_3}{1 - \gamma_1 \gamma_0} \tag{33}$$

Let

$$\tilde{\Delta}(t) := \begin{bmatrix} \tilde{\Delta}_1 & 0 \\ 0 & B_2^+ (I + MB_1 B_2^N B_2^+)^{-1} (I + \tilde{\Delta}_2) \end{bmatrix} \tag{34}$$

and so, by construction, $\tilde{\Delta}(t)$ from Eq. (34) satisfies:

$$\|\tilde{\Delta}(t)\| < \frac{\gamma_0 \gamma_3}{1 - \gamma_1 \gamma_0} \tag{35}$$

Proposition 1: During a fault or failure condition, for any combination of $0 < w_i \leq 1$, the closed-loop system will be stable if

$$0 < \frac{\gamma_2 \gamma_0 \gamma_3}{1 - \gamma_1 \gamma_0} < 1 \tag{36}$$

where

$$\gamma_2 = \|\tilde{P}(s)\|_\infty \tag{37}$$

Proof: Consider the reduced-order system from Eq. (28), rewritten as follows,

$$\dot{\hat{e}}_1(t) = \tilde{A}_{11} \hat{e}_1(t) + [\tilde{G} \quad -B_1 B_2^N] \tilde{u}(t) \tag{38}$$

$$\tilde{y}(t) = \begin{bmatrix} \tilde{H} \\ \tilde{A}_{21} \end{bmatrix} \hat{e}_1(t) \tag{39}$$

where

$$\tilde{u}(t) := \tilde{\Delta}(t) \tilde{y}(t) \tag{40}$$

Then, clearly

$$\tilde{y}(s) = \tilde{P}(s) \tilde{u}(s) \tag{41}$$

where $\tilde{P}(s)$ is defined in Eq. (29) and, from the small gain theorem (Khalil [47]), if

$$\|\tilde{P}(s)\|_\infty \|\tilde{\Delta}(s)\| < 1 \tag{42}$$

then the closed-loop system in Eqs. (38–41) is stable. Using Eqs. (29) and (35) yields

$$\|\tilde{P}(s)\|_\infty \|\tilde{\Delta}(s)\| < \frac{\gamma_2 \gamma_0 \gamma_3}{1 - \gamma_1 \gamma_0} \tag{43}$$

and so, if Eq. (36) holds, then from the inequality equation (43), the small gain condition in Eq. (42) is satisfied, and the proposition is proved. QED

Remark: The γ_1 and γ_2 depend on the particular choice of the sliding surface matrix M. Crucially though, they do not depend on the weight W. Conversely, γ_0 depends on W but not on the design matrix M. The scalar γ_3 introduced in this paper depends on the uncertainty in the system matrix when structural damage occurs. Equation (36) represents a test to guarantee the stability of the closed-loop system when faults occur (i.e., when the w_i vary). One important feature is that, in order for Eq. (26) to hold, the norm of the pseudoinverse B_2^+, which depends on W, must be bounded for all $0 < w_i \leq 1$ (which is shown in Eq. (20) and was proved in Alwi and Edwards [16] and Stewart [46]).

For a given design of hyperplane, γ_1 and γ_2 are fixed. The gain γ_0 is independent of the control design and depends on the faults and the input distribution matrix. The magnitude of the uncertainty γ_3, which can be tolerated, must be such that

$$\gamma_3 \leq \frac{1 - \gamma_1 \gamma_0}{\gamma_2 \gamma_0} = \frac{1}{\gamma_2} \left(\frac{1}{\gamma_0} - \gamma_1 \right) \tag{44}$$

Because $\gamma_3 \geq 1$, a necessary condition is that

$$\frac{\gamma_2 \gamma_0}{1 - \gamma_1 \gamma_0} < 1 \tag{45}$$

which is the condition in Alwi and Edwards [16].

Remark: Note that the condition $\|MB_1 B_2^N B_2^+\| < 1$, which guarantees the inverse in Eq. (25) exists, holds because

$$\|MB_1 B_2^N B_2^+\| \leq \|MB_1 B_2^N\| \|B_2^+\| \leq \gamma_1 \gamma_0 < 1$$

The scalar γ_0 depends on W (but not on M) and can be interpreted physically as a worst-case upper bound on the change in the feedback loop gain in Eqs. (40) and (41), resulting from the faults. The scalar γ_1 depends on the designed M (i.e., the choice of sliding surface), but it is independent of W. Therefore, during the control law design cycle, if $\gamma_1 \gamma_0 < 1$ is not satisfied, M (which is chosen to make $\hat{A}_{11} - \hat{A}_{12}M$ stable) needs to be redesigned (for example, by lowering the performance requirements).

B. Sliding Mode Control Law

Next, a sliding mode controller will be designed based on the system in Eq. (23) with respect to the virtual control $\nu(t)$. The proposed control law is given by

$$\nu(t) = \nu_l(t) + \nu_n(t) \tag{46}$$

where

$$\nu_l(t) := -\tilde{A}_{21} \hat{e}_1(t) - \tilde{A}_{22} \sigma(t) + \nu_m(t) \tag{47}$$

and $\nu_m(t)$ is defined in Eq. (12). The nonlinear component is defined to be

$$\nu_n(t) := -[\rho(t) + \eta] \frac{\sigma(t)}{\|\sigma(t)\|} \tag{48}$$

for

$$\sigma(t) \neq 0$$

where η is a positive scalar.

Remark: During implementation, the discontinuity in the nonlinear control term $\sigma(t)/\|\sigma(t)\|$ has been smoothed by using a sigmoidal approximation $\sigma(t)/[\|\sigma(t)\| + \delta]$, where δ is a small fixed positive scalar (see, for example Chapter 3.7 in Edwards and Spurgeon [44]). This removes the so-called chattering effect in the

control signal and introduces further degrees of tuning to accommodate the actuator rate limits (especially during actuator fault or failure conditions).

It follows that the actual control that is sent to the actuators is resolved from the virtual control law $v(t)$ [from Eqs. (47) and (48)], using Eqs. (4) and (5). Therefore, $u(t)$ is defined as

$$u(t) = B_2^T v(t) \tag{49}$$

Provided Eq. (36) is satisfied, the sliding mode controller can handle total actuator failures in the original system in the situation when $\det(B_2 W B_2^T) \neq 0$. Standard sliding mode controllers cannot handle total actuator failures, although their inherent robustness can cope with faults.

In a fault-free situation, it is not necessary and, indeed, is not advisable to have a large gain on the switched term; therefore, ideally, the term $\rho(t)$ should adapt to the onset of a fault and react accordingly. It is easy to see from Eq. (47) that, if $y_d(t)$ is bounded, $v_l(t)$ is bounded by

$$\|v_l(t)\| < l_1 \|e(t)\| + l_2 \tag{50}$$

where l_1 and l_2 are known positive constants. The gain from Eq. (48) is defined to be

$$\rho(t) = r(t)(\bar{r}_1 \|e(t)\| + \bar{r}_2) \tag{51}$$

where

$$\bar{r}_1 := [\gamma_4 + (2 + \gamma_1) l_1]; \qquad \bar{r}_2 := [\gamma_5 + (2 + \gamma_1) l_2] \tag{52}$$

and the constants γ_4 and γ_5 are defined as

$$\gamma_4 := \|\tilde{A}_2^{\delta} T_\sigma T_r\|, \qquad \|A_2^{\delta} \tilde{x}_m\| \leq \gamma_5 \tag{53}$$

where A_2^{δ}, T_σ, and T_r are defined in Eqs. (24), (22), and (15), respectively. The scalar variable $r(t)$ is an adaptive gain that varies according to

$$\dot{r}(t) = a(\bar{r}_1 \|e(t)\| + \bar{r}_2) D_\epsilon(\|\sigma(t)\|) - b r(t) \tag{54}$$

where $r(0) = 0$, and the a and b are positive design constants. The function D_ϵ: $\mathbb{R} \mapsto \mathbb{R}$ is the nonlinear function,

$$D_\epsilon(\|\sigma\|) = \begin{cases} 0 & \text{if } \|\sigma\| < \epsilon \\ \|\sigma\| & \text{otherwise} \end{cases} \tag{55}$$

where ϵ is a positive scalar. Here, ϵ is fixed to be small and helps define a boundary layer about the surface $\mathcal{S}$, inside which an acceptably close approximation to ideal sliding takes place. Provided the states evolve with time inside the boundary layer, no adaptation of the switching gains takes place. If a fault occurs, which starts to make the sliding motion degrade so that the states evolve outside the boundary layer (i.e., $\|\sigma(t)\| > \epsilon$), then the dynamic coefficients $r(t)$ increase in magnitude [according to Eq. (54)] to force the states back into the boundary layer around the sliding surface. The choice of the design parameters η, a, b, and ϵ depends on the closed-loop performance specifications and requires some design iteration. The choice of these design parameters will be discussed further in Sec. V. The following proposition will show that $r(t)$ is bounded, and motion inside a boundary layer around $\mathcal{S}$ is obtained.

Define $\mathcal{W}$ to be the set of faults, such that

$$\mathcal{W} = \{(w_1, \ \ldots, \ w_{n_u}) \in \underbrace{[0, \ 1] \times \ \cdots \ \times [0, \ 1]}_{n_u \text{times}} | \underline{\lambda}(B_2 W B_2^T) := w > 0\} \tag{56}$$

where w is a strictly positive scalar, and $\underline{\lambda}(B_2 W B_2^T)$ represents the smallest eigenvalue of $(B_2 W B_2^T)$. Notice that

$$(w_1, \ \ldots, \ w_{n_u}) \in \mathcal{W} \Rightarrow \det(B_2 W B_2^T) \neq 0$$

Proposition 2: Consider the potentially faulty system represented by Eq. (1) with the control law in Eqs. (47) and (48); then, the adaptive gain $r(t)$ from Eqs. (51–55) remains bounded, and the switching states $\sigma(t)$ enter a boundary layer around $\mathcal{S}$ in finite time for any fault condition $(w_1, \ \ldots, \ w_{n_u}) \in \mathcal{W}$.

Proof: See Appendix.

Remark: Close approximation to ideal sliding can be maintained, even in the presence of faults for an appropriate choice of a, b, and ϵ. If $\epsilon = 0$ and $b = 0$, it follows that $\dot{V} \leq -w^2 \|\sigma\|(1 - \gamma_1 \gamma_0)\eta$, which means that ideal sliding can be attained and maintained in finite time. However, $\epsilon = 0$ is not a practical choice because, in the presence of noise, for example, $r(t)$ may become unbounded.

V. Controller Design

The main objective of the controller design is to bring the damaged El Al 1862 aircraft to a near-landing condition on runway 27 at Schiphol Airport (through a proper landing approach, using LOC and glide-slope (GS) capture procedures). It is assumed that no FDI or fault reconstruction is available that replicates the actual El Al 1862 scenario; the flight crew were even unaware that engine nos. 3 and 4 had detached from the right wing.

A linearization of the nominal aircraft has been obtained around an operating condition of 263×10^3 kg (560×10^3 lb), 92.6 m/s (180 kt) true airspeed, and an altitude of 600 m (2000 ft) at 25.6% of maximum thrust and at a 20 deg flap position. The result is a 12th-order linear model (separated into two sixth-order models) associated with the lateral and longitudinal states. For design purposes, only the four longitudinal ($x_{\text{long}} = [\,q \quad V_{\text{tas}} \quad \alpha \quad \theta\,]^T$) and lateral states ($x_{\text{lat}} = [\,p \quad r \quad \beta \quad \phi\,]^T$) have been retained. The lateral control surfaces are

$$\delta_{\text{lat}} = [\delta_{\text{air}} \ \ \delta_{\text{ail}} \ \ \delta_{\text{aor}} \ \ \delta_{\text{aol}} \ \ \delta_{\text{sp1-4}} \ \ \delta_{\text{sp5}} \ \ \delta_{\text{sp8}} \ \ \delta_{\text{sp9-12}} \ \ \delta_r \ \ e_{1_{\text{lat}}} \ \ e_{2_{\text{lat}}} \ \ e_{3_{\text{lat}}} \ \ e_{4_{\text{lat}}}]^T$$

which represent aileron deflection (right and left/inboard and outboard) (rad), spoiler deflections (left: 1–4 and 5, right: 8 and 9–12) (rad), rudder deflection (rad), and lateral engine pressure ratios (EPRs). The longitudinal control surfaces are

$$\delta_{\text{long}} = [\,\delta_e \quad \delta_s \quad e_{1_{\text{long}}} \quad e_{2_{\text{long}}} \quad e_{3_{\text{long}}} \quad e_{4_{\text{long}}}\,]^T$$

which represent elevator deflection (rad), horizontal stabilizer deflection (rad), and longitudinal EPR.

The controlled outputs represent the stated roll ϕ and sideslip angle β, for lateral control, and the FPA and speed V_{tas}, for longitudinal control. These linear models of the nominal-damage free aircraft will be used to design the control schemes, which will be described in the next sections. This is a major difference when compared with Maciejowski and Jones [9], in which the MPC controller is designed based on exact knowledge of the postdamage aircraft.

In the original coordinates, the linear component of the control law can be summarized as

$$v_l(t) = Le(t) + Fx_m(t) + Gy_d(t)$$

where $L = -SA$, and SB_v has been scaled so that $SB_v = I$. The nonlinear term $v_n(t)$ is given in Eq. (48), where the nonlinear gain $\rho(t)$ is based on the adaptive law in Eqs. (51–55).

A. Lateral Controller Design

The feedback matrices for the ideal lateral model from Eq. (12) have been designed using eigenstructure assignment (Liu and Patton [48]). The eigenvalues were chosen as $\{-0.3500 \pm 0.1500, \ -0.5000, \ -0.4000\}$, and the desired and obtained eigenstructures are, respectively,

$$\underbrace{\begin{bmatrix} *+*i & *-*i & * & 0 \\ 0 & 0 & 0 & 0 \\ *+*i & *-*i & 0 & 0 \\ 1+*i & 1-*i & 1 & 1 \end{bmatrix}}_{\text{desired}}$$

$$\longrightarrow \underbrace{\begin{bmatrix} 0.3195-0.1369i & 0.3195+0.1369i & 0.4498 & 0.3748 \\ -0.0000-0.0000i & -0.0000+0.0000i & -0.0430 & -0.0526 \\ 0.1619+0.1412i & 0.1619-0.1412i & 0.0182 & 0.0275 \\ -0.9127 & -0.9127 & -0.8919 & -0.9252 \end{bmatrix}}_{\text{obtained}}$$

The feedforward matrix G_{lat} has been designed using the inverse steady-state gain for the virtual triple $(A_{\text{lat}}, B_{\nu_{\text{lat}}}, C_{c_{\text{lat}}})$; specifically,

$$G_{\text{lat}} = -[C_{c_{\text{lat}}}(A_{\text{lat}} + B_{\nu_{\text{lat}}}F_{\text{lat}})^{-1}B_{\nu_{\text{lat}}}]^{-1}$$

It will be assumed that at least one of the control surfaces for both ϕ and β tracking will be available when a fault or failure occurs (i.e., one of either the four ailerons or the four spoilers will be available, and one of either the rudder or the four engine thrusts are available). Under these assumptions, a numerical search yields that the scalar from Eq. (20) is $\gamma_{0_{\text{lat}}} = 8.1314$.

Next, the matrix M, which defines the hyperplane, must be computed so that the conditions of Eq. (36) are satisfied. Here, a quadratic optimal design (Edwards and Spurgeon [44]) has been used to obtain S_{lat} [which depends on the matrix M_{lat} in Eq. (21)]. The state weighting matrix has been chosen as $Q_{\text{lat}} = \text{diag}(2, 2, 1, 1)$. The poles associated with the reduced-order sliding motion are $\{-0.7136 \pm 0.0522i\}$, and the associated natural frequency and damping ratio are 0.7155 and 0.9973, respectively. Based on M_{lat}, it can be shown that $\gamma_{1_{\text{lat}}}$ from Eq. (30) satisfies $\gamma_{1_{\text{lat}}} = 0.0230$. Consequently, $\gamma_{0_{\text{lat}}}\gamma_{1_{\text{lat}}} = 0.1870 < 1$, and the requirements of Eq. (36) are satisfied. For the case of the El Al 1862 scenario, and by using $\tilde{G}_{\text{lat}} = 0.001I_2$ and $\tilde{H}_{\text{lat}} = I_2$ (which allow perturbations in all elements of $\tilde{A}_{11}$), it was found that the norm from Eq. (31) is $\gamma_{3_{\text{lat}}} = 1.5134$.

Finally, it can be verified that the $\mathcal{H}_\infty$ norm from Eq. (37) is $\|\tilde{P}_{\text{lat}}(s)\|_\infty = \gamma_{2_{\text{lat}}} = 0.0589$. Therefore, from Eq. (36),

$$\frac{\gamma_{2_{\text{lat}}}\gamma_{0_{\text{lat}}}\gamma_{3_{\text{lat}}}}{1-\gamma_{1_{\text{lat}}}\gamma_{0_{\text{lat}}}} = 0.8916 < 1$$

which shows that the system is stable for all $0 < w_i \leq 1$. For implementation, the discontinuity in the nonlinear control term in Eq. (48) has been smoothed by using a sigmoidal approximation, $\nu^{\delta}_{n,\text{lat}} = \sigma_{\text{lat}}/(\|\sigma_{\text{lat}}\| + \delta_{\text{lat}})$, where the scalar $\delta_{\text{lat}} = 0.05$. This introduces further DOF to accommodate actuator rate limits.

For simplicity, the variables related to the adaptive nonlinear gain have been chosen as $\bar{r}_{1_{\text{lat}}} = 0$ and $\bar{r}_{2_{\text{lat}}} = 1$. The parameter η_{lat}, from Eq. (48), was chosen as $\eta_{\text{lat}} = 1$. In practice, a maximum limit $\rho_{\max}$ for the adaptive nonlinear gain in Eq. (51) has been imposed to avoid the actuators becoming too aggressive. Here, the maximum gain was set at $\rho_{\max_{\text{lat}}} = 5$. The adaptation parameters from Eq. (54) have been chosen as $a_{\text{lat}} = 100$, $b_{\text{lat}} = 0.01$, and $\epsilon_{\text{lat}} = 5 \times 10^{-2}$. The parameter ϵ_{lat} was chosen to be able to tolerate the variation in $\|\sigma_{\text{lat}}(t)\|$ due to normal changes in flight conditions, but it was chosen to be small enough to enable the adaptive gain to be sensitive to deviations from zero due to faults or failures. Here, a_{lat} has been chosen to be large to enable small changes in $\|\sigma_{\text{lat}}(t)\|$ to cause significant changes in the gain, so that the control system reacts quickly to a fault. The parameter b_{lat}, on the other hand, dictates the rate at which $\rho_{\text{lat}}(t)$ will decrease after $\|\sigma_{\text{lat}}(t)\|$ has returned below the threshold ϵ_{lat}.

To emulate real aircraft-flight-control capability, an outer-loop heading control law was designed, based on a proportional–integral derivative (PID) controller, to provide a roll command to the inner-loop sliding mode controller. In the SIMONA implementation, this outer-loop heading control can be activated by a switch in the cockpit. The proportional gain was $K_{p_{\text{lat}}} = 3$, the integrator gain was set as $K_{i_{\text{lat}}} = 0.1$, and the derivative gain was set as $K_{d_{\text{lat}}} = 3$. Note that the integrator component is only activated when the heading angle error is less than 5 deg to remove unwanted oscillation during maneuvers but to still eliminate steady-state error.

B. Longitudinal Controller Design

As in the lateral controller, the feedback matrices for the ideal longitudinal model from Eq. (12) have been designed using eigenstructure assignment. The eigenvalues were chosen as $\{-0.2400 \pm 0.1700,\ -0.7000,\ -0.1250\}$, and the desired and obtained eigenstructures are

$$\underbrace{\begin{bmatrix} 0.5+*i & 0.5-*i & 0 & 0 \\ 0 & 0 & 0 & 1 \\ 0.5+*i & 0.5-*i & 0 & 0 \\ 0 & 0 & 1 & 0 \end{bmatrix}}_{\text{desired}}$$

$$\longrightarrow \underbrace{\begin{bmatrix} 0.1812-0.1283i & 0.1812+0.1283i & -0.1057 & 0.0001 \\ -0.0020+0.0015i & -0.0020-0.0015i & -0.0060 & 1.0000 \\ 0.3220-0.5264i & 0.3220+0.5264i & 0.9829 & -0.0037 \\ -0.7549 & -0.7549 & 0.1510 & -0.0012 \end{bmatrix}}_{\text{obtained}}$$

As in the lateral controller design, the feedforward matrix G_{long} has been designed using the inverse steady-state gain for the virtual triple, so that

$$G_{\text{long}} = -[C_{c_{\text{long}}}(A_{\text{long}} + B_{\nu_{\text{long}}}F_{\text{long}})^{-1}B_{\nu_{\text{long}}}]^{-1}$$

It will be assumed that at least one of the control surfaces for FPA tracking will still be available when a fault or failure occurs. It is also assumed that at least one of the four engines is available for V_{tas} tracking. Under these assumptions, a numerical search yields $\gamma_{0_{\text{long}}} = 8.2913$.

As in the lateral controller, a quadratic optimal design has been used to obtain the sliding surface matrix. The weighting matrix defining the cost has been chosen as $Q_{\text{long}} = \text{diag}(2, 2, 1, 1)$. The poles associated with the sliding motion can be shown to be $\{-1.1157,\ -0.3737\}$ (the associated natural frequencies and damping ratios are 0.6457 and 1.1533, respectively). For this choice of surface, it can be shown that $\gamma_{1_{\text{long}}} = 3.0160 \times 10^{-4}$ and $\gamma_{0_{\text{long}}}\gamma_{1_{\text{long}}} = 0.0025 < 1$. Consequently, the requirements of Eq. (36) are satisfied. For the case of the El Al 1862 scenario, with $\tilde{G}_{\text{long}} = 0.001I_2$ and $\tilde{H}_{\text{long}} = I_2$, the norm from Eq. (31) is $\gamma_{3_{\text{long}}} = 1.3842$. Finally, it can be shown that the $\mathcal{H}_\infty$ norm from Eq. (37) is $\|\tilde{P}_{\text{long}}(s)\|_\infty = \gamma_{2_{\text{long}}} = 0.0115$. Consequently, from Eq. (36),

$$\frac{\gamma_{2_{\text{long}}}\gamma_{0_{\text{long}}}\gamma_{3_{\text{long}}}}{1-\gamma_{1_{\text{long}}}\gamma_{0_{\text{long}}}} = 0.1319 < 1$$

This shows that the system is stable for all $0 < w_i \leq 1$. The discontinuity in the nonlinear control term in Eq. (48) has been smoothed by using a sigmoidal approximation, $\nu^{\delta}_{n,\text{long}} = \sigma_{\text{long}}/(\|\sigma_{\text{long}}\| + \delta_{\text{long}})$, where the scalar $\delta_{\text{long}} = 0.05$.

As in the lateral design, the variables related to the adaptive nonlinear gain have been chosen as $\bar{r}_{1_{\text{long}}} = 0$ and $\bar{r}_{2_{\text{long}}} = 1$. This was also found to give sufficiently good performance, remove the dependence of $r(t)$ on $e(t)$, and simplify the implementation. The parameter η_{long} from Eq. (48) was chosen as $\eta_{\text{long}} = 1$. In practice, a maximum limit $\rho_{\max}$ for the adaptive nonlinear gain in Eq. (51) is imposed to restrain the actuators from becoming too aggressive. Here, the maximum gain was set as $\rho_{\max_{\text{long}}} = 2$. The adaptation parameters from Eq. (54) have been chosen, similar to those in the lateral design (i.e., $a_{\text{long}} = 100$, $b_{\text{long}} = 0.01$, and $\epsilon_{\text{long}} = 5 \times 10^{-2}$).

Again, to emulate real aircraft-flight-control capability, an outer-loop altitude control law was designed, based on a PID, to provide a FPA command to the inner-loop sliding mode controller. In the SIMONA implementation, this outer-loop altitude control can be

activated by a switch in the cockpit. The proportional gain was set as $K_{p_{\text{long}}} = 0.001$, the integrator gain was set as $K_{i_{\text{long}}} = 0.00004$, and the derivative gain was set as $K_{d_{\text{long}}} = 0.02$. Note that the integrator component is only activated when the altitude error is less than 15 m to remove unwanted oscillation during maneuvers and to eliminate steady-state error.

As a result of the architecture employed, both the lateral and longitudinal controllers manipulate the EPRs. In the trials, control mixing was employed, in which the signals from both the lateral controller and the longitudinal controller were added together before being applied to each of the engines. This is similar to the approach adopted in Burcham et al. [4].

Remark: In terms of the control law design, no actuator magnitude or rate saturations are accounted for explicitly. However, in the evaluations on SIMONA, these effects are present. The model-reference tracking framework was purposely chosen in this paper, because it does not suffer from windup problems (due to the absence of integrators). In the event a rate limit or position limit is exceeded, a difference between the expected actuator position and the commanded one occurs, which would be interpreted as a fault. The robustness property of sliding mode controllers to actuator faults would then mitigate the effect of the saturation by increasing the control effort deployed in the remaining available actuators through the control allocation process, thus reducing the burden on the saturated actuator.

VI. Test Pilot Results

The designed controller was implemented on the SIMONA flight simulator. The command inputs from the pilot are regulated through the MCP. In this control scheme, an approach (APP) button on the MCP is implemented, which is engaged in order to intercept the LOC and GS for the desired runway. The controller was implemented as a SIMULINK model, with appropriate inputs and outputs to connect it with the SIMONA hardware, as shown in Fig. 4. In Fig. 4, an ILS landing capability has been added to the control loop to allow the aircraft to land on runway 27 at Schiphol. The controller was set up to work with an ODE4 solver with a fixed time step of 0.01 s. The available processing power is sufficient to run the controller in real time (i.e., within 10 ms per time step). A connection with the MCP on the flight deck enables the selection of control modes (e.g., altitude hold, heading select, and reference values). The simulator trials were performed with the speed, altitude, and heading select modes active. The pilot commands new headings, speeds, or altitudes by adjusting the controls on the MCP.

Remark: The proposed controller is relatively, simple because it is designed from a linearization about an operating condition. The controller presented in this paper is considered to be a proof of concept to show the capabilities of combining SMC and CA. It will be shown in the sequel that, despite being designed from a linearization, the controller is able to give good performance over a relatively large flight envelope, even in the presence of very significant and damaging faults. Because it is developed from a linearization, the controller has a relatively simple structure and is not computationally intensive. This enabled the controller to be implemented on SIMONA in real time, within the 0.01 s update time window necessary for implementation, as described in Smaili et al. [27] and Stroosma et al. [12].

A. ILS Landing

A sensor that measures the deviation from the LOC angle/beam error (which is available in typical transport aircraft) combined with the current aircraft heading is used for aligning the aircraft toward the runway. The output of this outer loop is a roll demand for the LOC controller and an FPA demand for the GS controller. These demand signals replace the pilot's commands to the main SMC controller to allow for an almost automatic landing procedure. The outer-loop controller (LOC and GS) is armed by the pilot by engaging the APP button on the MCP when the aircraft is near the LOC signal coverage (see Fig. 4 for details). In normal operation, the LOC will be the first to be engaged (LOC valid) when the aircraft is inside the LOC coverage [for this implementation, the distance measurement equipment (DME) is less than 46.3 km when the aircraft is inside the coverage angle of ± 10 deg from the LOC beacon and (-7 deg, -0.75 deg) inside the GS beacon]. During the armed phase, the LOC controller is in standby mode, and the aircraft is controlled by either heading or roll commands from the pilot. When the LOC is engaged (LOC valid), the LOC controller will provide the inner roll command to the core lateral sliding mode controller, and the whole process becomes an automatic landing mode (i.e., no input from the pilot is needed). The GS is then engaged (GS valid) when the aircraft is inside the GS coverage [i.e., the DME is less than 18.5 km, the LOC is within ± 8 deg, and the GS is within (-1.35 deg, -5.25 deg) inside coverage]. The GS is in an armed phase (after the APP button is engaged), and the GS controller is in a standby mode, with the aircraft controlled using altitude or via FPA commands from the pilot. When the GS controller is engaged (GS valid), the GS controller will provide the FPA command to the core longitudinal SMC controller; again, no input from the pilot is needed. If, for some reason, during the LOC and GS maneuver to the runway, the LOC or GS becomes invalid (i.e., if the aircraft goes outside the LOC and GS coverage cones), the outer-loop controller commands revert to heading and altitude hold (and the LOC and GS controllers provide zero roll and FPA commands, respectively: see Fig. 4). Then, the pilot can retake full control of the aircraft by disengaging the APP mode.

Note that the reference command for ϕ was limited to 15 deg, and a 0 deg reference was applied for β to force a slide-slip free flight. As described in Lombaerts et al. [11], a postfailure safe-flight-envelope analysis suggests that a safe roll maneuver can only be achieved for demand values of less than 20 deg. However, it can be argued that, based on the current controller implemented in the B747, the roll reference from the autopilot is limited for passenger comfort, and especially for LOC turning maneuvers during the final stages of all ILS landings. Having conservative roll capabilities is a plausible predesign assumption when designing controllers for faults or failure conditions.

B. Flight Simulator Results with Experienced Pilots

The controller has been flown by three different pilots (airline and test pilots) with experience on B747, B767, A330, and Citation II aircraft. An experienced B767 and Citation II pilot had rigorously tested the controller during the flight evaluation campaign before the GARTEUR FM–AG16 final workshop in November 2007. During the final workshop, an experienced B747 pilot flew the damaged aircraft on the SIMONA simulator, during a presentation to the general public that included the local Dutch press (television news, radio, and newspapers). The results presented here are from tests flown by an experienced A330 pilot and a test pilot for the National Aerospace Laboratory, The Netherlands during the pilot evaluation campaign in November 2007.

Note that, even though the controller has been designed based on the linearization using a mass of approximately 263,000 kg at a 20 deg flap position, the controller was tested with a heavy trim mass of 317,000 kg at a 1 deg flap position, as per the actual El Al 1862 aircraft. This removes the advantage of low-mass and low-speed maneuverability and higher performance and controllability when compared with the heavy trim mass, which was one of the main findings in Smaili and Mulder [8]. The heavy trim mass for the flight test also replicates the actual El Al 1862 scenario and fits with the assumption that the exact damage and condition of the aircraft, postfaults, is unknown, thus making the challenge even harder.

The flight test was executed as realistically as possible. As in the actual El Al 1862 scenario, the aircraft flew in a northerly direction from runway 01L before starting to make a right turn. Immediately after the right turn, the El Al failure scenario occurs (see Fig. 5), whereby engine nos. 3 and 4 detach from the right wing and cause significant damage to the right wing. The objective is to fly the damaged aircraft back to the runway, as intended by the crew of El Al 1862. The chosen runway, runway 27, faces west at an angle of

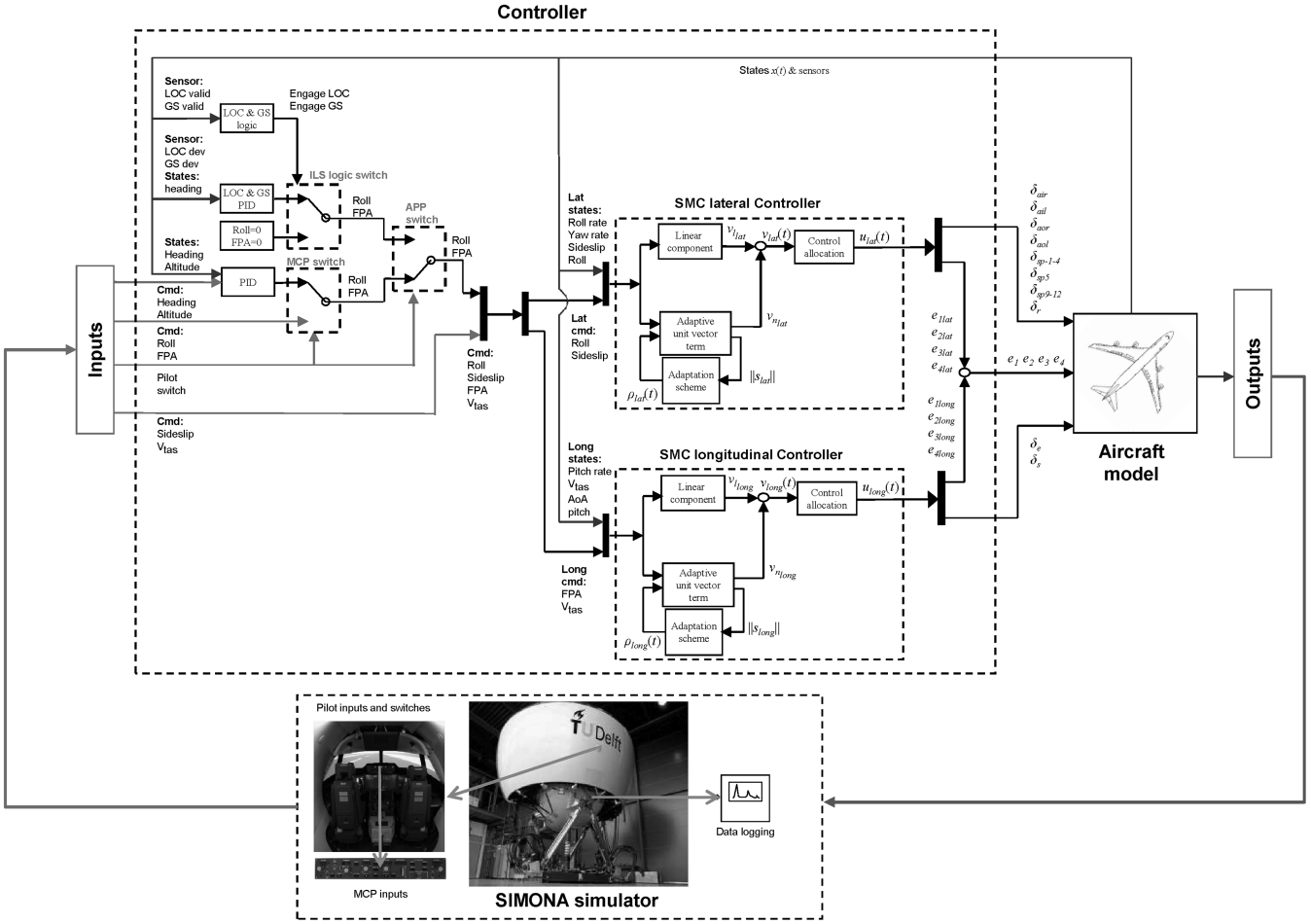

Fig. 4 SIMONA interconnections (cmd denotes command signal).

approximately 269 deg from the north. Therefore, in order for the aircraft to land, two 90 deg turns must be performed before aligning the aircraft on runway 27. During the third right turn, the aircraft is required to capture a LOC signal, which guides the heading of the aircraft to line it up with the runway. During this normal procedure for landing, the aircraft will also be required to intercept a GS signal to enable the aircraft to descend at a 3 deg FPA, which will bring the aircraft to the landing target zone. The flare and the actual landing of the aircraft are not carried out, and the simulation was stopped at a point 50 ft above ground level.

C. Classical Controller

Figure 5 shows the results of the piloted evaluation using the classical controller and proposed SMC controller. The idea of a fault-free test of the SMC is to give the pilot the feel of the capability of the controller in the nominal condition. Initially, the aircraft was flown straight and level before a heading change of 90 deg to the east was performed. The pilot tested the aircraft's capability to climb to a prespecified altitude, from a 600 m (2000 ft) altitude to approximately 800 m (2500 ft). Then, the pilot commands a return to an altitude of 600 m and performs another right turn to capture the LOC. At this stage, the pilot arms the approach mode in order to prepare for an automated landing approach. Once the aircraft captures the LOC signal, a final turn toward the centerline of runway 27 is started and, after the GS signal is captured, the aircraft descends toward the runway at a 3 deg GS. Note that, starting from the moment the pilot activates the APP button in the MCP and the LOC signal has been captured, the aircraft is in a fully automated landing mode, and no other pilot input is required.

The classical controller was also tested by the pilots to give them some feel of the severity of the actual El Al scenario. With this controller, the pilots manually flew the aircraft using control wheel and column inputs. Piloted evaluation using the classical controller under the El Al 1862 scenario (Fig. 5) shows that, after the failure, the aircraft is still able to do right turns. Only during the final stage of the test flight does the aircraft lose control and crash before being able to line up with the runway.

Figures 6–8 show the results of the piloted evaluation using the classical controller tested under the El Al flight 1862 scenario.

Figure 6 shows the pilot control deflections. As described in the studies in Smaili and Mulder [8] and the incident report [29], similar patterns appear. Immediately after the failure, the deflection of the wheel, column, and pedal increase in magnitude. As in the El Al 1862

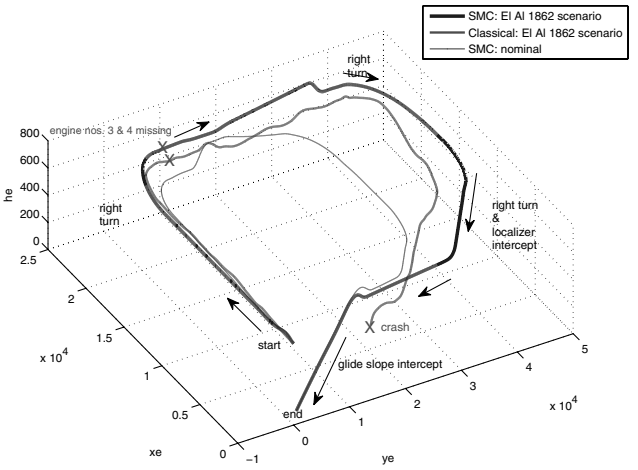

Fig. 5 Classical and SMC controller: three-dimensional flight trajectory.

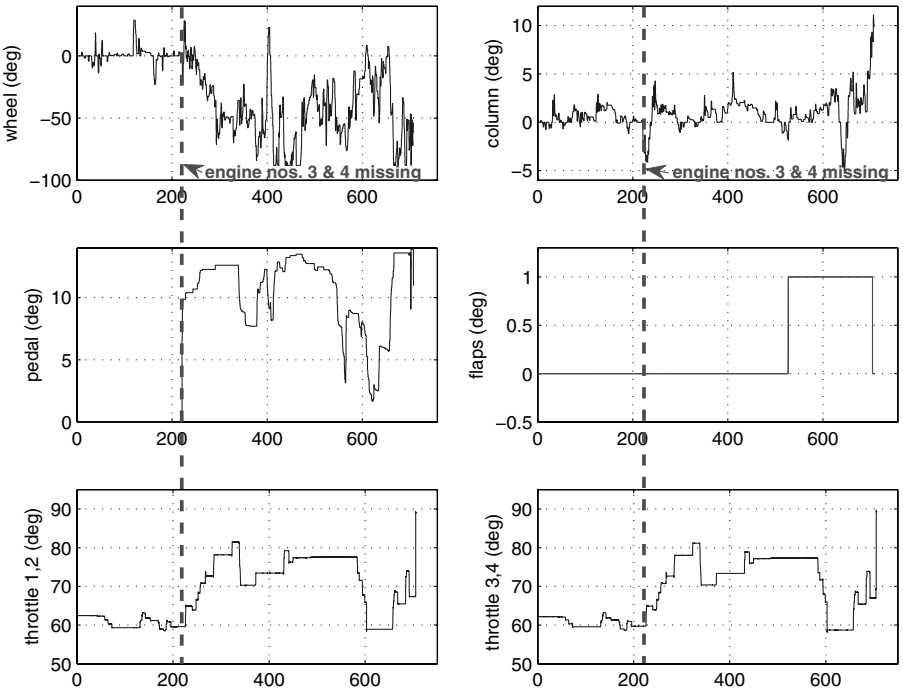

Fig. 6 El Al 1862 scenario with classical controller: pilot deflection.

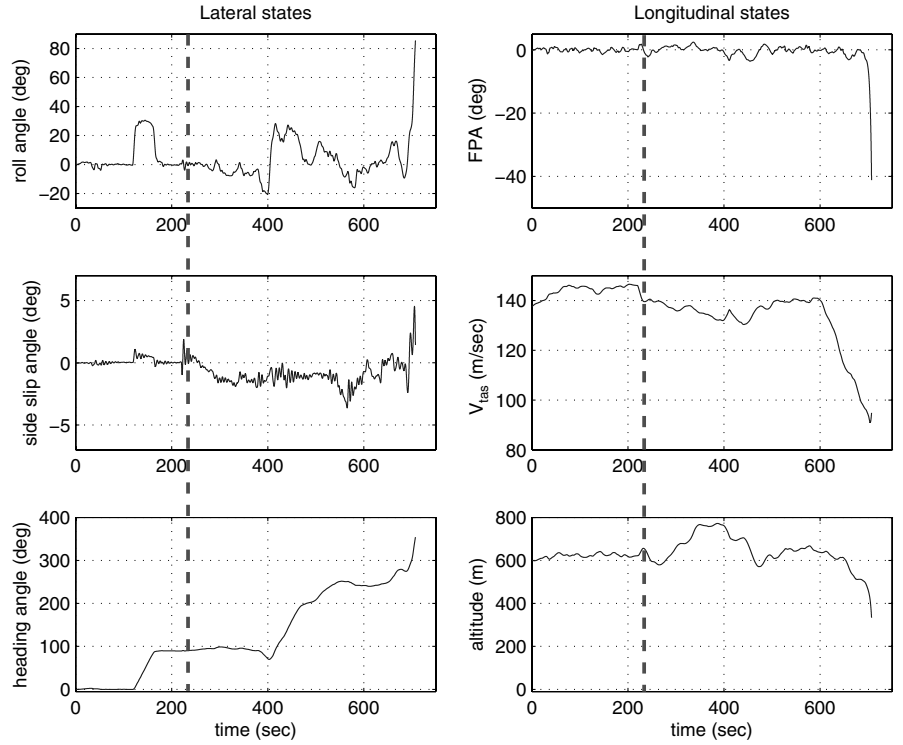

a) Controlled states

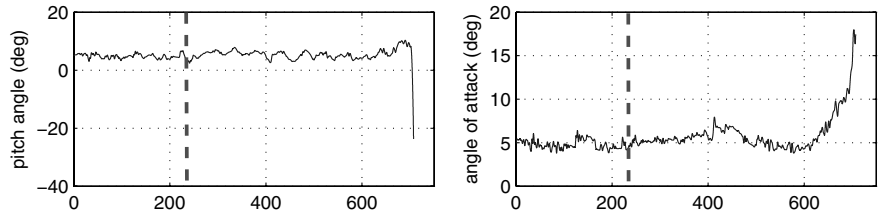

b) Pitch angle and angle of attack

Fig. 7 El Al 1862 scenario with classical controller: states.

flight, almost maximum wheel deflection to the left (negative) to counter the right turn is visible. Also visible is the pedal deflection to counteract the yawing moment of the asymmetric thrust. Figure 6 also shows that, near to the final stages of the test, a flap setting of 1 deg is selected to prepare for landing. At about 600 s, the power lever angle (throttle) is also reduced for landing. However, when the speed reaches 110 m/s (approximately 220 kt) near 700 s (Fig. 7), the aircraft becomes hard to control and banks to the right. Figure 6 shows that maximum left (negative) pilot wheel deflection is applied. Still unable to recover from the right bank, the flap is returned to a 0 deg setting, and the throttle input is increased in order to regain control. However, the aircraft still rolls to the right and loses altitude and speed. The loss of altitude and FPA tries to be compensated by the high positive (pull toward the pilot) column deflection. At this stage, all control is lost, and the aircraft rolls at almost 80 deg right, with the FPA nearing −40 deg and the pitch angle passing −20 deg. This is similar to what is described in the incident report in [29], when the El Al 1862 aircraft hit the apartment building in Bijlmermeer, Amsterdam.

Analyzing the plots further, it can be seen that, when the throttle is reduced in preparation for landing, the speed becomes low and, during descent, the angle of attack becomes high. As discussed in the incident report [29] and Smaili et al. [8,27], the increase in the angle of attack causes (high) flow separation and turbulence behind the damaged right-wing leading edge, resulting in the loss of lift and drag (compared with the left wing). This increases the rolling and yawing moment to the right and a further drop in altitude and speed.

Figure 8 shows the control surface deflections of the classical controller. One major feature of the classical controller is that most of the control surfaces are mechanically linked. For example, the outboard ailerons on the left and right wing are only fully active when a flap setting of more than 5 deg is used (Hanke and Nordwall [49] and Hanke [50]). This can be seen in Fig. 8, in which the outboard aileron is inactive (0 deg deflection) throughout the flight test. The large deflection of the left aileron and spoilers up to the saturation limits (−20 deg for the aileron and 40 deg for the spoiler) after the engine failure show that there is limited control, even at a speed of 130–140 kt. Note that a positive deflection for ailerons is a deflection down, and for the spoilers, positive is deflected up (Hanke and Nordwall [49] and Hanke [50]). Figure 8 shows that the aileron deflections are, most of the time, at the saturation limits after the loss of engine nos. 3 and 4, to provide a roll moment in order to obtain straight and level flight; therefore, most of the roll maneuver capability is assisted by the left spoiler deflections. Shortly after the reduction in speed (i.e., approximately after 600 s), the left aileron and spoilers saturate again, due to the lower speed and higher angle of attack, the control surface deflections are insufficient to regain control, as the aircraft has gone beyond the capability of the control surfaces to provide enough roll moment. Note that the general control surface deflections and behavior in Figs. 6–8 closely follow the findings of the actual El Al 1862 incident reported by the Netherlands Aviation Safety Board [29].

Figure 5 shows the flight trajectory of the test. Three different trajectories are shown: the El Al 1862 scenario with classical and SMC controllers and one with the SMC without any failure. With the classical controller, the pilot manages to maintain some performance and managed two banking-turn maneuvers. During the preparation for landing and capture of the LOC, the aircraft loses control, and the simulation is stopped. The other two trajectories associated with safe landings by the SMC controller will be discussed in the next section.

D. Sliding Mode Controller

As discussed in Sec. V, the controller has been designed based on a linearization obtained around an operating condition of 263×10^3 kg (580×10^3 lb), 92.6 m/s (180 kt) true airspeed, and an altitude of 600 m (2000 ft) at 25.6% of maximum thrust and at a 20 deg flap position. The actual pilot tests were performed at 317×10^3 kg (700×10^3 lb), a speed of 133.8 m/s (260 kt), and a flap setting of 1 deg. The tests were deliberately undertaken at a different trim condition to allow the pilot to rigorously test the controller and access its performance under different operating conditions.

Note that, for the purpose of testing the modern FTC strategies, the large transport aircraft setup in the GARTEUR FM–AG16 program, using the FTLAB747 software, has been modified to include a state-of-the-art fly by wire (FBW) capability, removing mechanical links and locks from the classical B747 configuration (Smaili et al. [27]). This allows more flexibility in the control strategy, exploiting independent control of all available surfaces, thus increasing the ways redundant control surfaces can be used to achieve FTC.

Figure 5 also shows the trajectory of the SMC controller tested with the El Al 1862 failure scenario. The same controller as that

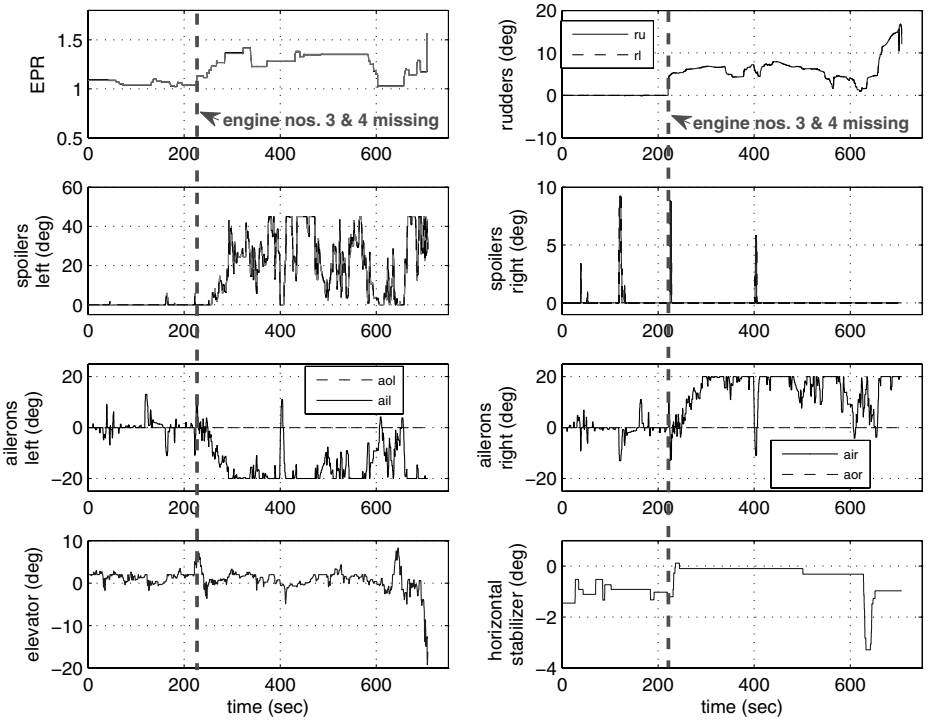

Fig. 8 El Al 1862 scenario with classical controller: control surface deflection (ru denotes upper rudder, and rl denotes lower rudder).

used in the nominal fault-free case is applied. In general, the controller performs the same right-turn maneuvers, LOC and GS intercept, and lands on runway 27. The SMC with the El Al 1862 failure manages to bring the aircraft near to landing on the desired runway. Figure 9 shows the controlled states of the damaged aircraft with the SMC controller. Note at the beginning of the simulation, before the failure occurs at around 200 s, the FPA, V_{tas}, and altitude show small steady-state errors due to the mismatch between the designed trim conditions and the test conditions, as described earlier. This is due to the absence of integrators in the main SMC controller. The mismatch between the designed and test trim conditions demonstrates the controller coping with uncertainty and allows the pilot to rigorously test the controller outside its comfort zone.

Figure 9 shows that, after the failure occurs at approximately 200 s, the climb capability of the aircraft is severely degraded when the pilot requests an increase in altitude to 800 m (from 600 m). On the other hand, the more important descent capability of the SMC controller is not degraded, as it is able to follow the GS of 3 deg toward the runway. This is shown in Fig. 10. The GS error is maintained below 0.5 deg. Figure 9 shows that the sideslip angle of the damaged aircraft has been maintained in the interval (0.5 deg, -1.5 deg), which is an improvement on the classical controller (as flown by the pilot) in Fig. 9. Heading changes of the damaged aircraft with the SMC controller in Fig. 9 also show a more systematic and higher level of performance, even when subjected to the El Al 1862 failures. This shows that the lateral controller is able to deal with the asymmetrical thrust condition, extensive wing damage, and control surface loss of efficiency (due to the failure of hydraulic systems 3 and 4), and it maintains the desired change in heading. Decreasing the speed [to approximately 120 m/s (233.26 kt)] helps in terms of lateral control (Smaili and Mulder [8] and the incident report [29]). This is due to the lower thrust that is required at lower speed, and thus a lower yawing moment results from the asymmetrical thrust condition. This is seen in terms of the deviation of the sideslip angle in Fig. 9. The sideslip angle is much smaller than at a higher speed after the failure has occurred. The roll angle tracking again shows good performance, even after the loss of the engines and the hydraulics associated with the El Al 1862 scenario.

Note that, in Fig. 9, the heading angle and altitude plot only show the command signals from the MCP. After the LOC and GS have been engaged, the heading and altitude commands from the MCP are no longer used (and remain at the set value). Instead, the heading and altitude commands come from the ILS navigation (not shown in the heading angle and altitude plot in Fig. 9).

Figure 10 shows the signals from the ILS sensors. It represents the DME, LOC, and GS deviations and the moment when the LOC and the GS are valid/engaged after being armed using the APP button in the MCP. As usual, the LOC is engaged before the GS. The LOC coverage is much further than the GS, and this allows the aircraft to be aligned to the extended centerline of the runway before following the specified 3 deg GS descent.

Figure 11 shows the control surface deflections under the El Al 1862 scenario. This figure highlights the major difference between the classical controller (which is mechanically linked) and the FBW aircraft that has been provided by the GARTEUR FM-AG16 modification (Smaili et al. [27]). In this figure, the outboard ailerons can be seen to be independently mobile before the occurrence of the failure. After the failure, the right outboard ailerons float due to the loss of hydraulic systems 3 and 4. Independent control can also be seen in the spoilers, elevators, rudders, and EPR. The effect of losing the hydraulic system can also be seen in the floating of the inboard left and outboard right elevators (see Fig. 11), for which a clear distinction between the control surface deflection can also be seen. The spoilers also show similar patterns. Before the losses of engine nos. 3 and 4 occurred, all the spoilers seemed to be moving independently and, when the failure occurs, only spoilers 2, 3, 10, and 11 are active; the rest remain at zero deflection. In general, the control surface deflections of the elevators, ailerons, and spoilers are almost half of the ones using the classical controller (see Fig. 11). The control surface deflections from the SMC controller do not reach the saturation limits of the surfaces, and the spoilers and the ailerons are generally less aggressive. Engine EPR shows that differential thrust has been used to achieve the desired performance: to obtain a small sideslip and roll angle. Note that all the surfaces are controlled independently by the CA SMC scheme. Pilot's inputs only come from supplying the higher-level commands, such as heading and altitude change (or roll or FPA commands through the MCP panel).

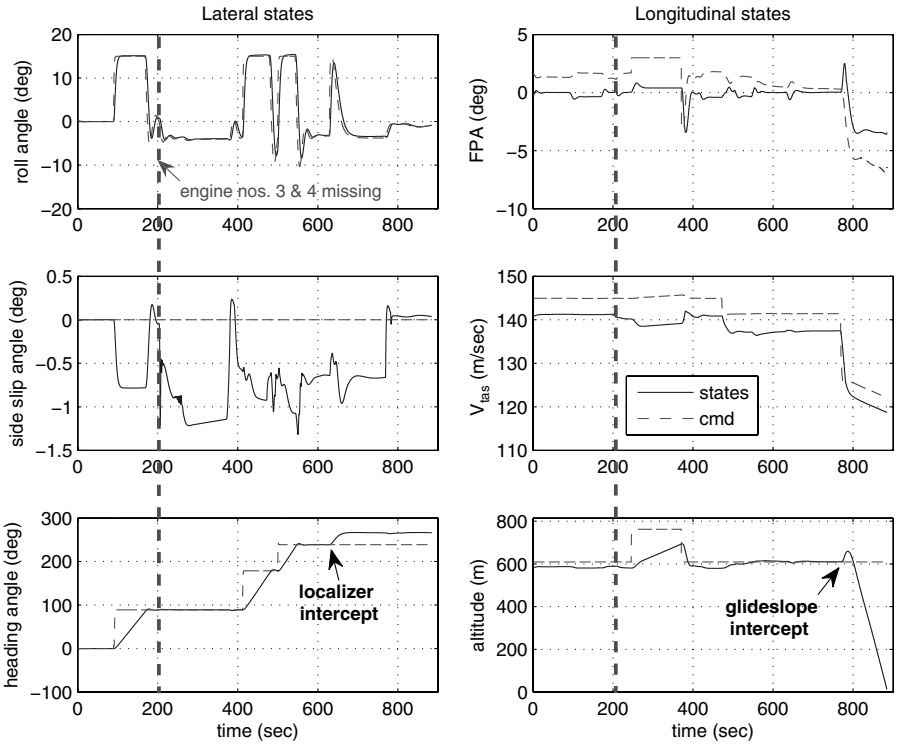

Fig. 9 El Al 1862 scenario with SMC controller: controlled states.

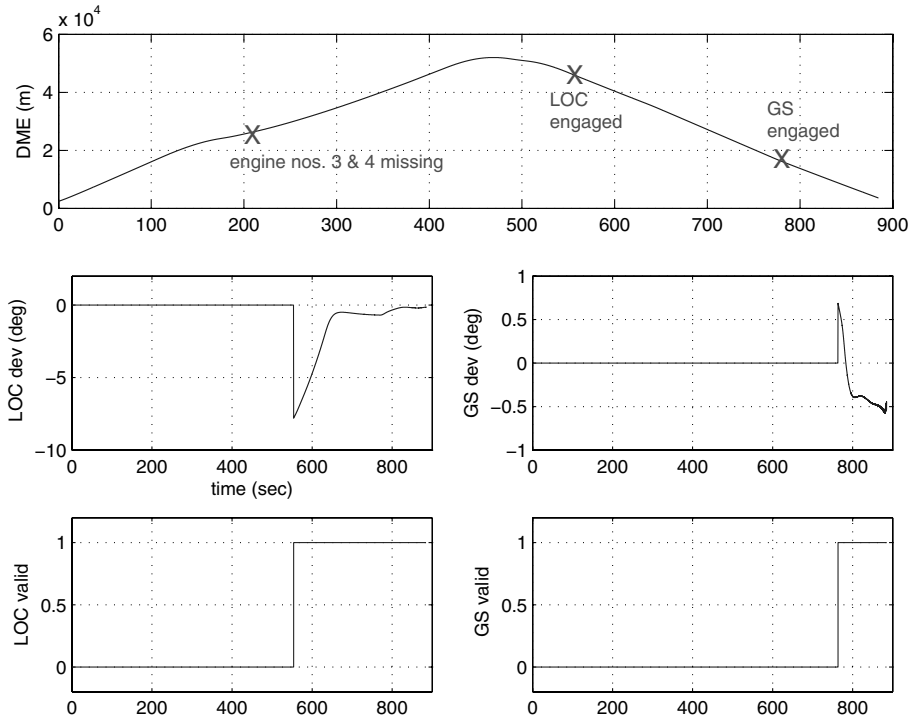

Fig. 10 El Al 1862 scenario with SMC controller: LOC and GS deviation angles.

This reduces the pilot's workload in comparison with the classical controller, for which the demand is high.

Remark: Fig. 11 shows no chattering in the lateral and longitudinal control surface deflections, because the discontinuity in the nonlinear control term in Eq. (48) has been smoothed by using a sigmoidal approximation, as explained in Sec. V. Figure 11 shows that the right outboard aileron has an up (negative) deflection due to the float failure, resulting from the loss of hydraulics. During a float failure (as described in Bošković and Mehra [51]), the control surface moves freely without producing any moment. In the case of straight and level flight, the floating control surface moves freely in the direction of the angle of attack (Ganguli et al. [52]) [i.e., at an up (negative) position]. Note that, although during the design stage the elevator is modeled as one surface, as shown in Fig. 11, the robustness property of SMC (to uncertainty in the actuator channels) and the flexibility of the CA scheme manage to redistribute the control effort to the remaining functional elevators (i.e., the left outboard and right inboard elevators) and the stabilizer.

Figures 12a and 12b show the adaptive gain and the associated $\|\sigma(t)\|$ signals that initiate the gain adaptation. Before the occurrence

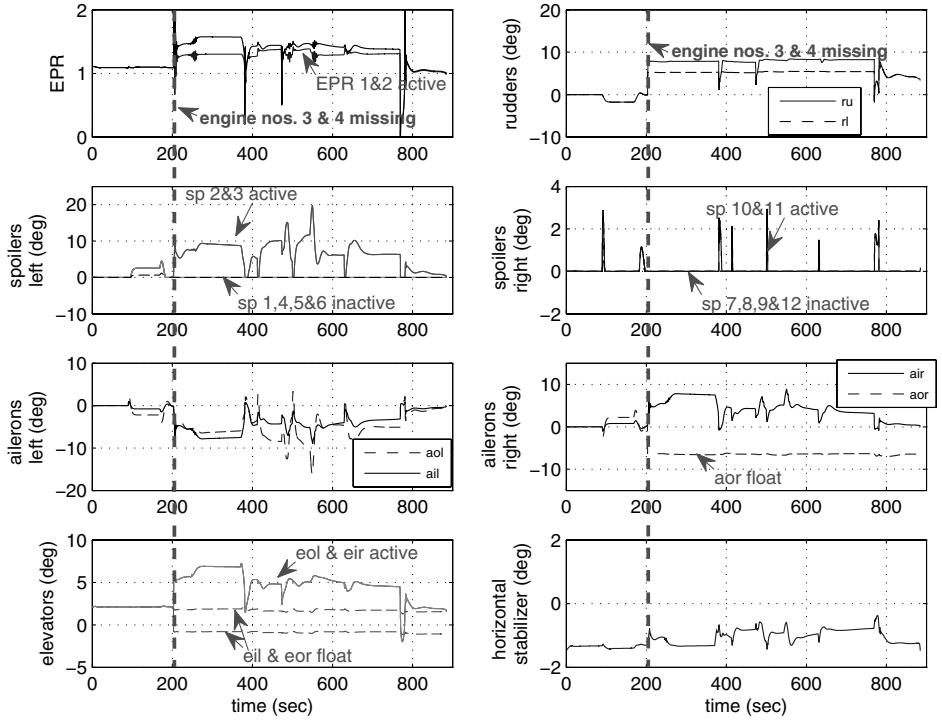

Fig. 11 El Al 1862 scenario with SMC controller: control surface deflection.

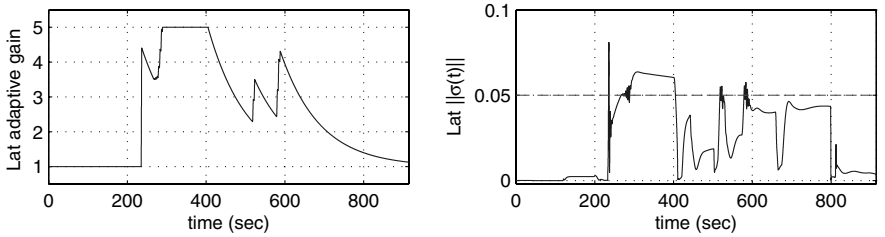

a) Lateral

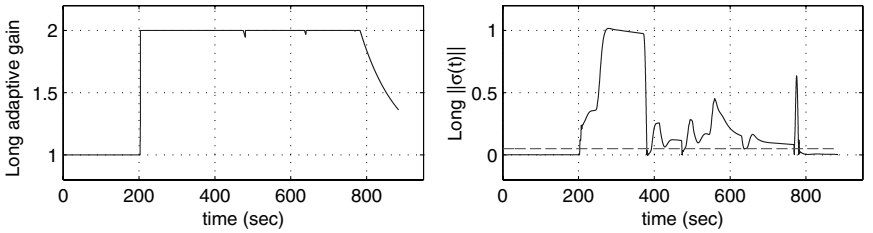

b) Longitudinal

Fig. 12 El Al 1862 scenario with SMC controller: adaptive gain and switching function.

of the failure, the sliding signal $\sigma(t)$ is below the selected threshold. Once the threshold is exceeded, the gain is adapted from a minimum of one, up to the maximum of five, and two for the lateral and longitudinal axes, respectively. A large deviation from the sliding surface $\sigma(t) = 0$ shows the severity of the faults. After the failure has occurred, and during maneuvers, the switching function plot $\sigma(t)$ deviates away from the ideal sliding surface. However, during- or near-landing conditions, the switching function returns below the adaptation threshold, near to zero. During this time, the adaptive gain reduces to the minimum value of one.

Although the SMC controller can be implemented in such a way that the pilot's inputs (such as column, wheel, and pedal) can also be used, the purpose here is to show that, as a proof of concept, the SMC controller is more than able to handle all the rigorous tests and failures it is subjected to, using the minimal amount of input from the pilot, thus lowering the workload during such an emergency condition. This allows the pilot to concentrate on higher-level decisions.

VII. Conclusions

This paper has presented piloted flight simulator results associated with the El Al flight 1862 (Bijlmermeer incident) scenario, which is one of the case studies of the GARTEUR FM-AG16. The results represent the successful implementation of a FTC SMC controller on the SIMONA 6-DOF flight simulator, configured to represent a large transport aircraft with pilots evaluating and testing the controller. The results show that the proposed SMC scheme has the ability to position an aircraft for landing. This paper has further developed the SMC allocation scheme proposed in Alwi and Edwards [15,16] to handle the situation in which changes to the nominal system matrix occur as a result of damage to the airframe, which changes the aerodynamic properties of the aircraft. A formal proof of closed-loop stability has been provided for a range of parameter variations.

Appendix

Proof of Proposition 2: Define a scalar:

$$\zeta := \frac{1}{w^2(1-\gamma_1\gamma_0)} \tag{A1}$$

The expression for ζ in Eq. (A1) is guaranteed to be positive because, in the requirements of Eq. (36), the inequality $\gamma_1\gamma_0 < 1$ must hold. Assume that $\dot{K}(t) = 0$ almost always; this implies $\dot{W}(t) = 0$ almost always, and so only isolated abrupt step changes in the effectiveness are considered here. Using the fact that $(B_2WB_2^T) > 0$, the following candidate Lyapunov function,

$$V = \frac{1}{2}\left\{\sigma^T(B_2WB_2^T)\sigma + \frac{w^2}{a}(1-\gamma_1\gamma_0)[r(t)-\zeta]^2\right\} \tag{A2}$$

is positive definite with respect to σ, the adaptive gain error $r(t) - \zeta$, and is radially unbounded. Taking derivatives along trajectories,

$$\dot{V} = \sigma^{\mathrm{T}}(B_2WB_2^T)\dot{\sigma} + \frac{w^2}{a}(1-\gamma_1\gamma_0)(r(t)-\zeta)\dot{r}(t) \tag{A3}$$

From Eq. (23) [and using Eqs. (46) and (47)],

$$\begin{aligned}\dot{\sigma}(t) &= (\tilde{A}_{21} + \tilde{A}_{21}^{\delta})\hat{e}_1(t) + (\tilde{A}_{22} + \tilde{A}_{22}^{\delta})\sigma(t) + [\nu(t) - \nu_m(t)] \\ &\quad - (I - MB_1B_2^NWB_2^T - B_2WB_2^T)\nu(t) + \tilde{A}_2^{\delta}\tilde{x}_m(t) \\ &= \tilde{A}_{21}^{\delta}\hat{e}_1(t) + \tilde{A}_{22}^{\delta}\sigma(t) + (I + MB_1B_2^NB_2^+)(B_2WB_2^T)\nu_n(t) \\ &\quad - (I - MB_1B_2^NWB_2^T - B_2WB_2^T)\nu_l(t) + \tilde{A}_2^{\delta}\tilde{x}_m(t) \\ &= \tilde{A}_2^{\delta}\tilde{e}(t) + \tilde{A}_2^{\delta}x_m(t) + (I + MB_1B_2^NB_2^+)(B_2WB_2^T)\nu_n(t) \\ &\quad - (I - MB_1B_2^NWB_2^T - B_2WB_2^T)\nu_l(t)\end{aligned} \tag{A4}$$

where $\tilde{e} = \mathrm{col}[\hat{e}_1(t),\ \sigma(t)]$. Using the fact that

$$\begin{aligned}\|\tilde{A}_2^{\delta}\tilde{e}(t) + \tilde{A}_2^{\delta}x_m(t)\| &\le \|\tilde{A}_2^{\delta}\tilde{e}(t)\| + \|\tilde{A}_2^{\delta}\tilde{x}_m(t)\| \\ &\le \underbrace{\|\tilde{A}_2^{\delta}T_{\sigma}T_r\|}_{\gamma_4}\|e(t)\| + \underbrace{\|\tilde{A}_2^{\delta}\tilde{x}_m(t)\|}_{\gamma_5}\end{aligned} \tag{A5}$$

and

$$\sigma(t)^T(B_2WB_2^T)(B_2WB_2^T)\sigma(t) = \|B_2WB_2^T\sigma\|^2$$

where $\|(B_2WB_2^T)\| \le \|B_2B_2^T\| = 1$, together with the fact that $\|WB_2^T\| \le \|W\|\|B_2^T\| \le 1$ for all $(w_1, \ldots, w_{n_u}) \in \mathcal{W}$, it follows that, when $\sigma \neq 0$,

$$\begin{aligned}\sigma^T(B_2WB_2^T)\dot{\sigma} &= -\frac{(\rho+\eta)}{\|\sigma\|}\|B_2WB_2^T\sigma\|^2\\ &\quad -(\rho+\eta)\sigma^T(B_2WB_2^T)(MB_1B_2^NB_2^+)(B_2WB_2^T)\frac{\sigma}{\|\sigma\|}\\ &\quad -\sigma^T(B_2WB_2^T)(I-MB_1B_2^NWB_2^T-B_2WB_2^T)\nu_l(t)\\ &\quad +\sigma^T(B_2WB_2^T)[\tilde{A}_2^\delta\tilde{e}(t)+\tilde{A}_2^\delta\tilde{x}_m(t)]\\ &\le -\frac{(\rho+\eta)}{\|\sigma\|}\|B_2WB_2^T\sigma\|^2\\ &\quad +\frac{(\rho+\eta)}{\|\sigma\|}\|B_2WB_2^T\sigma\|^2\|(MB_1B_2^NB_2^+)\|\\ &\quad +\|B_2WB_2^T\sigma\|\|(I-MB_1B_2^NWB_2^T-B_2WB_2^T)\|\|\nu_l(t)\|\\ &\quad +\|B_2WB_2^T\sigma\|\|(\tilde{A}_2^\delta\tilde{e}(t)+\tilde{A}_2^\delta\tilde{x}_m(t))\|\\ &\le \|B_2WB_2^T\sigma\|\Bigg[-\frac{(\rho+\eta)}{\|\sigma\|}\|B_2WB_2^T\sigma\|(1-\gamma_1\gamma_0)\\ &\quad +(2+\gamma_1)\|\nu_l(t)\|+(\gamma_4\|e(t)\|+\gamma_5)\Bigg] \end{aligned} \tag{A6}$$

because

$$\|MB_1B_2^NB_2^+\| \le \|MB_1B_2^N\|\|B_2^+\| \le \gamma_0\gamma_1$$

and

$$\begin{aligned}&\|I-MB_1B_2^NWB_2^T-B_2WB_2^T\|\\ &\quad \le 1+\|MB_1B_2^NWB_2^T\|+\|B_2WB_2^T\| \le 2+\gamma_1\end{aligned}$$

Using the Rayleigh principle,

$$-\|B_2WB_2^T\sigma\|^2 \le -\underline{\lambda}(B_2WB_2^T)^2\|\sigma\|^2 = -w^2\|\sigma\|^2$$

This, together with the fact that $\bar{\lambda}(B_2WB_2^T)=1$, means inequality equation (A6) implies

$$\begin{aligned}\sigma^T(B_2WB_2^T)\dot{\sigma} &\le -w^2\|\sigma\|(\rho+\eta)(1-\gamma_1\gamma_0)\\ &\quad +\|\sigma\|(2+\gamma_1)\|\nu_l(t)\|+\|\sigma\|[\gamma_4\|e(t)\|+\gamma_5]\\ &= w^2\|\sigma\|(1-\gamma_1\gamma_0)[-(\rho+\eta)+\zeta(2+\gamma_1)\|\nu_l(t)\|\\ &\quad +\zeta(\gamma_4\|e(t)\|+\gamma_5)]\\ &\le w^2\|\sigma\|(1-\gamma_1\gamma_0)\{-(\rho+\eta)+\zeta(2+\gamma_1)[l_1\|e(t)\|+l_2]\\ &\quad +\zeta[\gamma_4\|e(t)\|+\gamma_5]\}\\ &= w^2\|\sigma\|(1-\gamma_1\gamma_0)\{-(\rho+\eta)+\zeta\underbrace{[\gamma_4+(2+\gamma_1)l_1]}_{\bar{r}_1}\|e(t)\|\\ &\quad +\zeta\underbrace{[\gamma_5+(2+\gamma_1)l_2]}_{\bar{r}_2}\}\end{aligned} \tag{A7}$$

where ζ is defined in Eq. (A1), and $\bar{r}_1$ and $\bar{r}_2$ are defined in Eq. (52). Using Eqs. (50) and (51), the previous inequality (A7) can be written as

$$\begin{aligned}\sigma^T(B_2WB_2^T)\dot{\sigma} &\le -w^2\|\sigma\|(1-\gamma_1\gamma_0)\eta - w^2\|\sigma\|\\ &\quad \times(1-\gamma_1\gamma_0)[\bar{r}_1\|e(t)\|+\bar{r}_2][r(t)-\zeta]\end{aligned} \tag{A8}$$

Finally, substituting Eqs. (54) and (A8) into Eq. (A3) yields:

$$\begin{aligned}\dot{V} &\le -w^2\|\sigma\|(1-\gamma_1\gamma_0)\eta - w^2\|\sigma\|(1-\gamma_1\gamma_0)\\ &\quad \times[\bar{r}_1\|e(t)\|+\bar{r}_2][r(t)-\zeta]+w^2(1-\gamma_1\gamma_0)\\ &\quad \times[r(t)-\zeta][\bar{r}_1\|e(t)\|+\bar{r}_2]D_\epsilon(\|\sigma(t)\|)\\ &\quad -\frac{b}{a}w^2(1-\gamma_1\gamma_0)[r(t)-\zeta]r(t)\end{aligned} \tag{A9}$$

If $\|\sigma\|>\epsilon$, then $D_\epsilon(\|\sigma\|)=\|\sigma\|$, and so substituting in Eq. (A9) and simplifying terms yields:

$$\begin{aligned}\dot{V} &\le -w^2\|\sigma\|(1-\gamma_1\gamma_0)\eta-\frac{b}{a}w^2(1-\gamma_1\gamma_0)[r(t)-\zeta]r(t)\\ &\quad +\frac{b}{4a}\frac{1}{w^2(1-\gamma_1\gamma_0)}\end{aligned} \tag{A10}$$

By construction, $0\le\gamma_1\gamma_0<1$ and $r(t)\ge 0$. Further manipulation of Eq. (A10) and using Eq. (A1) yields,

$$\begin{aligned}\dot{V} &\le -w^2\|\sigma\|(1-\gamma_1\gamma_0)\eta-\frac{b}{a}w^2(1-\gamma_1\gamma_0)\left(\frac{1}{2}\zeta-r\right)^2\\ &\quad +\frac{b}{4a}\frac{1}{w^2(1-\gamma_1\gamma_0)}\end{aligned} \tag{A11}$$

because expanding the quadratic term on the right-hand side of Eq. (A11) gives the right-hand side of Eq. (A10). If $\|\sigma\|>\epsilon$, then

$$w^2\|\sigma\|(1-\gamma_1\gamma_0)\eta \ge w^2(1-\gamma_1\gamma_0)\eta\epsilon$$

The quantities ϵ, η, a, and b are design parameters, and so if they are chosen to satisfy

$$\epsilon\eta \ge \frac{b}{4a}\frac{1}{w^4(1-\gamma_1\gamma_0)^2}=\frac{b}{4a}\zeta^2 \tag{A12}$$

then from Eq. (A11),

$$\dot{V}\le -\frac{b}{a}w^2(1-\gamma_1\gamma_0)\left(\frac{1}{2}\zeta-r\right)^2\le 0$$

If $\|\sigma\|<\epsilon$, then $D_\epsilon(\|\sigma\|)=0$, and so substituting in Eq. (A9) and simplifying terms yields:

$$\begin{aligned}\dot{V} &\le -w^2\|\sigma\|(1-\gamma_1\gamma_0)\eta - w^2\|\sigma\|(1-\gamma_1\gamma_0)\\ &\quad \times[\bar{r}_1\|e(t)\|+\bar{r}_2][r(t)-\zeta]-\frac{b}{a}w^2(1-\gamma_1\gamma_0)[r(t)-\zeta]r(t)\end{aligned} \tag{A13}$$

Notice, by construction, $\gamma_1\gamma_0<1$ and $r(t)\ge 0$; therefore; for $\|\sigma\|<\epsilon$ and $r(t)>\zeta$, it follows $\dot{V}<0$. Define a rectangle in $\mathbb{R}^2$ as

$$\mathcal{R}=\{(\|\sigma\|,\ r)|\|\sigma\|\le\epsilon,\ 0\le r\le\zeta\} \tag{A14}$$

Also define $\mathcal{R}_+\in\mathbb{R}^2$ as $\mathcal{R}_+=\{(\|\sigma\|,\ r)|r\ge 0\}$. By construction of the adaptive gains, $r(t)\ge 0$ for all time, and so the trajectory of $(\|\sigma(t)\|,\ r(t))\in\mathcal{R}_+$ for all time, and so, outside the set $\mathcal{R}\cap\mathcal{R}_+=\mathcal{R}$, from Eqs. (A11) and (A13), the derivative of the Lyapunov function $\dot{V}<0$. Let $\mathcal{V}_d$ denote the truncated ellipsoid,

$$\mathcal{V}_d=\{(\|\sigma\|,\ r)|V(\|\sigma\|,\ r)\le d\}\cap\mathcal{R}_+$$

where $V(\cdot)$ is defined in Eq. (A2). Because $\mathcal{R}$ in Eq. (A14) is a compact set for a given $w>0$, there exists a unique $d_0>0$, such that $d_0=\min\{d\in\mathbb{R}_+|\mathcal{R}\subset\mathcal{V}_d\}$. As shown in Fig. A1, because $\mathcal{R}\subset\mathcal{V}_{d_0}$, it follows outside $\mathcal{V}_{d_0}$ that the derivative of the Lyapunov function $\dot{V}<0$, and so $\mathcal{V}_{d_0}$ is an invariant set that is entered in finite time t_0. Because $\mathcal{V}_{d_0}$ is entered in finite time, $V(\|\sigma\|,\ r)\le d_0$ for all $t>t_0$, which implies $\|\sigma\|\le\sqrt{2d_0/w}$ for $t>t_0$; hence, σ enters and remains in a boundary layer of size $\sqrt{2d_0/w}$ around the ideal sliding surface $\mathcal{S}$.

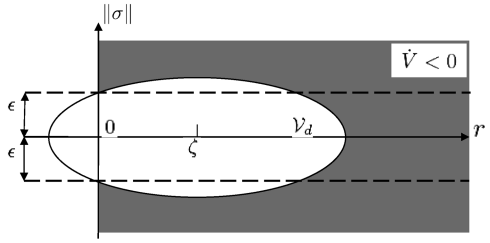

Fig. A1 Level set of the Lyapunov functions V.

References

[1] Burcham, F. W., Fullertron, C. G., and Maine, T. A., "Manual Manipulaton of Engine Throttles for Emergency Flight Control," NASA NASA/TM-2004-212045, 2004.

[2] Gero, D., *Aviation Disasters: The World's Major Civil Airliner Crashes Since 1950*, Patrick Stephens, Somerset, England, U.K., 2006.

[3] Burcham, F. W., Maine, T. A., Burken, J., and Bull, J., "Using Engine Thrust for Emergency Flight Control: MD-11 and B-747 Results," NASA TM 1998-206552, 1998.

[4] Burcham, F. W., Maine, T. A., Kaneshinge, J., and Bull, J., "Simulator Evaluation of Simplified Propulsion-Only Emergency Flight Control System on Transport Aircraft," NASA NASA/TM-1999-206578, 1999.

[5] Burcham, F. W., Burken, J., Maine, T. A., and Bull, J., "Emergency Flight Control Using Only Engine Thrust and Lateral Center-of-Gravity Offset: A First Look," NASA TM 4789, 1997.

[6] Tucker, T., "Touchdown: the Development of Propulsion Controlled Aircraft at NASA Dryden," Monographs in Aerospace History, No. 16, NASA, 1999.

[7] Burken, J., Burcham, J. W., Trindel, A. M., Feather, J., Goldthorpe, S., and Kahler, J., "Flight Test of Propulsion-Based Emergency Control System on the MD-11 Airplane with Emphasis on the Lateral Axis," NASA TM 4746, 1996.

[8] Smaili, M. H., and Mulder, J. A., "Flight Data Reconstruction and Simulation of the 1992 Amsterdam Bijlmermeer Airplane Accident," AIAA Modeling and Simulation Technologies Conference, AIAA Paper 2000-4586, 2000.

[9] Maciejowski, J. M., and Jones, C. N., "MPC Fault-Tolerant Control Case Study: Flight 1862," *Proceedings of the IFAC Symposium SAFEPROCESS '03*, Elsevier, New York, 2003, pp. 119–124.

[10] Hennig, A., and Balas, G. J., "MPC Supervisory Flight Controller: A Case Study to Flight EL AL 1862," AIAA Guidance, Navigation, and Control Conference and Exhibit, AIAA Paper 2008-6789, 2008.

[11] Lombaerts, T. J. J., Huisman, H. O., Chu, Q. P., Mulder, J. A., and Joosten, D. A., "Flight Control Reconfiguration Based on Online Physical Model Identification and Nonlinear Dynamic Inversion," AIAA Guidance, Navigation, and Control Conference and Exhibit, AIAA Paper 2008-7435, 2008.

[12] Stroosma, O., Smaili, H., Lombaerts, T., and Mulder, J. A., "Piloted Simulator Evaluation of New Fault-Tolerant Flight Control Algorithms for Reconstructed Accident Scenarios," AIAA Modeling and Simulation Technologies Conference and Exhibit, AIAA Paper 2008-6534, 2008.

[13] Shtessel, Y., Buffington, J., and Banda, S., "Tailless Aircraft Flight Control Using Multiple Time Scale Re-Configurable Sliding Modes," *IEEE Transactions on Control Systems Technology*, Vol. 10, No. 2, 2002, pp. 288–296. doi:10.1109/87.987075

[14] Wells, S. R., and Hess, R. A., "Multi-Input/Multi-Output Sliding Mode Control for a Tailless Fighter Aircraft," *Journal of Guidance, Control, and Dynamics*, Vol. 26, No. 3, 2003, pp. 463–473. doi:10.2514/2.5084

[15] Alwi, H., and Edwards, C., "Model-Reference Sliding Mode FTC With On-Line Control Allocation," *46th IEEE Conference on Decision and Control*, IEEE Publ., Piscataway, NJ, 2007, pp. 2639–2644.

[16] Alwi, H., and Edwards, C., "Fault Tolerant Control Using Sliding Modes with On-Line Control Allocation," *Automatica*, Vol. 44, No. 7, 2008, pp. 1859–1866. doi:10.1016/j.automatica.2007.10.034

[17] Alwi, H., Edwards, C., Stroosma, O., and Mulder, J. A., "Fault Tolerant Sliding Mode Control Design with Piloted Simulator Evaluation," *Journal of Guidance, Control, and Dynamics*, Vol. 31, No. 5, 2008, pp. 1186–1201. doi:10.2514/1.35066

[18] Patton, R. J., "Robustness in Model-Based Fault Diagnosis: The 1995 Situation," *Annual Reviews in Control*, Vol. 21, 1997, 2008, pp. 101–121. doi:10.1016/S1367-5788(97)00020-5

[19] Zhang, Y., and Jiang, J., "Bibliographical Review on Reconfigurable Fault Tolerant Control Systems," *Proceedings of the IFAC Symposium SAFEPROCESS '03*, Elsevier, New York, 2003, pp. 265–276.

[20] van der Linden, C. A. A. M., "DASMAT: Delft University Aircraft Simulation Model and Analysis Tool," Technical Univ. of Delft, TR LR-781, Delft, The Netherlands, 1996.

[21] Smaili, M. H., "FLIGHTLAB 747: Benchmark for Advance Flight Control Engineering," Technical Univ. Delft, TR, Delft, The Netherlands, 1999.

[22] Marcos, A., and Balas, G. J., "A Boeing 747-100/200 Aircraft Fault Tolerant and Diagnostic Benchmark," Univ. of Minnesota, Dept. of Aerospace and Engineering Mechanics, TR AEM-UoM-2003-1, 2003.

[23] Marcos, A., and Balas, G. J., "A Robust Integrated Controller/Diagnosis Aircraft Application," *International Journal of Robust and Nonlinear Control*, Vol. 15, No. 12, 2005, pp. 531–551. doi:10.1002/rnc.1010

[24] Marcos, A., Ganguli, S., and Balas, G. J., "An Application of H_∞ Fault Detection and Isolation to a Transport Aircraft," *Control Engineering Practice*, Vol. 13, No. 1, 2005, pp. 105–119. doi:10.1016/j.conengprac.2004.02.006

[25] Szaszi, I., Marcos, A., Balas, G. J., and Bokor, J., "Linear Parameter-Varying Detection Filter Design for a Boeing 747-100/200 Aircraft," *Journal of Guidance, Control, and Dynamics*, Vol. 28, No. 3, 2005, pp. 461–470. doi:10.2514/1.6689

[26] Zhou, K., Rachinayani, P. K., Liu, N., Ren, Z., and Aravna, J., "Fault Diagnosis and Reconfigurable Control for Flight Control Systems with Actuator Failures," *43rd IEEE Conference on Decision and Control*, IEEE Publ., Piscataway, NJ 2004, pp. 5266–5271.

[27] Smaili, M. H., Breeman, J., Lombaerts, T. J. J., and Joosten, D. A., "A Simulation Benchmark for Integrated Fault Tolerant Flight Control Evaluation," AIAA Modeling and Simulation Technologies Conference and Exhibit, AIAA Paper 2006-6471, 2006.

[28] Stroosma, O., van Paassen, M. M., and Mulder, M., "Using the SIMONA Research Simulator for Human–Machine Interaction Research," AIAA Modeling and Simulation Technologies Conference, AIAA Paper 2003-5525 , 2003.

[29] Anon, "EL AL Flight 1862, Aircraft Accident Report 92-11," The Netherlands Aviation Safety Board, TR 92-11, Hoofddorp, The Netherlands, 1994.

[30] Shin, D., Moon, G., and Kim, Y., "Design of Reconfigurable Flight Control System Using Adaptive Sliding Mode Control: Actuator Fault," *Proceedings of the Institution of Mechanical Engineers, Part G (Journal of Aerospace Engineering)*, Vol. 219, No. 4, 2005, pp. 321–328. doi:10.1243/095441005X30333

[31] Härkegård, O., and Glad, S. T., "Resolving Actuator Redundancy: Optimal Control vs Control Allocation," *Automatica*, Vol. 41, No. 1, 2005, pp. 137–144. doi:10.1016/S0005-1098(04)00255-9

[32] Härkegård, O., "Backstepping and Control Allocation with Applications to Flight Control," Ph.D. Thesis, Dept. of Electrical Engineering, Linköpings Univ., Linköping, Sweden, 2003.

[33] Beck, R. E., Application of Control Allocation Methods to Linear Systems with Four or More Objectives, Ph.D. Thesis, Virginia Polytechnic Inst. and State Univ., Blacksburg, VA, 2002.

[34] Horn, R., and Johnson, C., *Matrix Analysis*, Cambridge Univ. Press, New York, 1990, pp. 421.

[35] Penrose, R., "A Generalized Inverse for Matrices," *Proceedings of the Cambridge Philosophical Society (Mathematical and Physical Sciences)*, Vol. 51, No. 3, 1955, pp. 406–413. doi:10.1017/S0305004100030401

[36] Enns, D., "Control Allocation Approaches," *AIAA Guidance, Navigation and Control Conference and Exhibit*, AIAA, Reston, VA, 1998, pp. 98–108.

[37] Durham, W. C., "Constrained Control Allocation," *Journal of Guidance, Control, and Dynamics*, Vol. 16, No. 4, 1993, pp. 717–725. doi:10.2514/3.21072

[38] Landau, I., "Survey of Model-Reference Adaptive Techniques," *Automatica*, Vol. 10, No. 4, 1974, pp. 353–379. doi:10.1016/0005-1098(74)90064-8

[39] Landau, I., and Courtoil, B., "Design of Multivariable Adaptive Model-Following Control Systems," *Automatica*, Vol. 10, No. 5, 1974, pp. 483–494. doi:10.1016/0005-1098(74)90049-1

[40] Monopoli, R. V., and Subbarao, V. N., "Design of a Multivariable Model Following Adaptive Control System," *Proceedings of the 20th IEEE Conference on Decision and Control Including the Symposium on Adaptive Processes*, IEEE Publ., Piscataway, NJ, 1981, pp. 992–998.

[41] Broussard, J. R., and O'Brien, M. J., "Feedforward Control to Track the Output of a Forced Model," *IEEE Transactions on Automatic Control*, Vol. 25, No. 4, 1980, pp. 851–853. doi:10.1109/TAC.1980.1102409

[42] Zinober, A. S. I., El-Ghezawi, O. M. E., and Billings, S. A., "Multivariable Variable-Structure Adaptive Model-Following Control Systems," *IEE Proceedings D: Control Theory and Applications*, Vol. 129, No. 1, 1982, pp. 6–12.

[43] Utkin, V. I., *Sliding Modes in Control Optimization*, Springer–Verlag, Berlin, 1992, Chap. 3.

[44] Edwards, C., and Spurgeon, S. K., *Sliding Mode Control: Theory and Applications*, Taylor and Francis, Philadelphia, 1998, Chaps. 3–4.

[45] Alwi, H., and Edwards, C., "Sliding Mode FTC with On-Line Control Allocation," *45th IEEE Conference on Decision and Control*, IEEE Publ., Piscataway, NJ, 2006, pp. 5579–5584.

[46] Stewart, G. W., "On Scaled Projections and Pseudoinverses," *Linear Algebra and Its Applications*, Vol. 112, No. 1, 1989, pp. 189–193. doi:10.1016/0024-3795(89)90594-6

[47] Khalil, H., *Nonlinear Systems*, Prentice–Hall, Englewood Cliffs, NJ, 1992, Chap. 5.

[48] Liu, G. P., and Patton, R. J., *Eigenstructure Assignment for Control System Design*, Wiley, New York, 1998, Chap. 2.

[49] Hanke, C., and Nordwall, D., "The Simulation of a Jumbo Jet Transport Aircraft, Volume 2: Modelling Data," NASA CR-114494, 1970.

[50] Hanke, C., "The Simulation of a Large Jet Transport Aircraft, Volume 1: Mathematical Model," NASA CR-1756, 1971.

[51] Bošković, J. D., and Mehra, R. K., "Failure Detection, Identification and Reconfiguration in Flight Control," *Fault Diagnosis and Fault Tolerance for Mechatronic Systems: Recent Advances*, Springer–Verlag, New York, 2002, pp. 129–167.

[52] Ganguli, S., Marcos, A., and Balas, G. J., "Reconfigurable LPV Control Design for Boeing 747-100/200 Longitudinal Axis," *Proceedings of the American Control Conference*, Vol. 5, Nov. 2002, pp. 3612–3617. doi:10.1109/ACC.2002.1024489